Experimental Investigations on the Effect of Process Parameters of the 3D-Printing using Fused Deposition Modelling

A DISSERTATION

SUBMITTED IN PARTIAL FULFILMENT OF THE REQUIREMENTS
FOR THE AWARD OF DEGREE
OF

MASTER OF TECHNOLOGY

IN

PRODUCTION ENGINEERING

Submitted by-

JAWED ALAM

2K18/PIE/503

Under the supervision of

Prof. RANGANATH M. SINGARI **Head** **Department of Design**	**Dr. SHADAB AHMAD** **Guest Faculty** **Department of Design**

DEPARTMENT OF MECHANICAL ENGINEERING
DELHI TECHNOLOGICAL UNIVERSITY
(Formerly Delhi College of Engineering)
Bawana Road, Delhi -110042

AUGUST, 2021

DEPARTMENT OF MECHANICAL ENGINEERING
DELHI TECHNOLOGICAL UNIVERSITY
DELHI -110042

CANDIDATE'S DECLARATION

I, Jawed Alam, Roll No. 2K18/PIE/503, student of M.Tech (Production Engineering), hereby declare that project Dissertation titled "Experimental Investigation on the Effect of Process Parameters of the 3D-Printing using Fused Deposition Modelling", which is submitted by me Department of Mechanical Engineering, Delhi Technological University, Delhi, in partial fulfilment of the requirement for the award of the degree of Master of Technology, is original and not copied from any source without proper citation. This work has not previously formed the basis for the award of any degree, Diploma Associateship, fellowship or other similar title or recognition.

Place: Delhi

Date: JAWED ALAM

                                                                                         (2K18/PIE/503)

DEPARTMENT OF MECHANICAL ENGINEERING
DELHI TECHNOLOGICAL UNIVERSITY
Delhi -110042

CERTIFICATE

I hereby certify that project dissertation titled "Experimental Investigation on the Effect of Process Parameters of the 3D-Printing using Fused Deposition Modelling" which is submitted by JAWED ALAM, 2K18/PIE/503, Department of Mechanical Engineering, Delhi Technological University, Delhi in partial fulfilment of the requirement for the award of Degree of Master of Technology (Production Engineering) is a record of the project work carried out by student under my supervision. To the best of knowledge this work has not been submitted in any part or full for any degree or diploma to this university or elsewhere.

Place: Delhi

Date:

DR. RANGANATH M SINGARI

(Professor)

Department of Mechanical Engineering

Delhi Technological University

Delhi

DR. SHADAB AHMAD

(Guest Faculty)

Department of Design

Delhi Technological University

Delhi

ACKNOWLEDGEMENT

JAWED ALAM

(**2K18/PIE/503**)

M.Tech Production Engineering

Delhi Technological University, Delhi, India

ABSTRACT

This research work aims to model and predict Flexural strength and 0.2% offset yield strength of an acrylonitrile-butadiene-styrene (ABS) manufactured through 3D printing using FDM. This process been studied and optimised using a machine learning process. An artificial neural network (ANN) multi-parameter regression model was created and then input–output relations model developed by this network was optimised by genetic algorithm (GA) to avail optimised parameters. an L27 Taguchi array was used to combine the specific parameters (nozzle diameter, layer height, fill density, printing velocity, raster orientation and infill pattern) to perform experiments. All samples were subjected to a three-point bending test performed according to the ASTM D7264 standard aimed to obtain Flexural strength and the 0.2% offset yield strength. ANN models were highly optimized and provided a better approach for the prediction of higher values of E and $R_{P0.2}$ than their experimental. ANN-GA based modelling and optimization suggest a direct relation between choosing process parameters correctly and enhancing 3D- printing performance. ANN-GA approach provides a set of optimal solutions for obtaining suitable output values. Infill pattern plays a critical role in providing the strength. Patterns intermediated to linear, rectilinear and honeycomb can be suggested for desired Flexural strength and 0.2% offset yield strength within constraints of input factors.

CONTENTS

List of Figures

List of Tables

INTRODUCTION

1.1 Additive Manufacturing

Additive Manufacturing Several terms including additive fabrication, free form fabrication, direct part manufacturing, layered manufacturing refers to additive manufacturing (AM) [1]. According to ASTM designation, additive manufacturing is the process of joining materials to make objects from 3-D model data, usually layer upon layer, as opposed to subtractive manufacturing technologies [2]. Classification for additive manufacturing technologies is shown in **Figure 1.1** from [3]. AM technology classes are provided by these groups: binder jetting, material extrusion, directed energy deposition, powder bed fusion, material jetting, sheet lamination, and vat photopolymerization. Additive Manufacturing technologies enable the creation of geometrically complicated components and devices with graded material compositions that can be modified for the design and manufacturing of cellular structures [3].
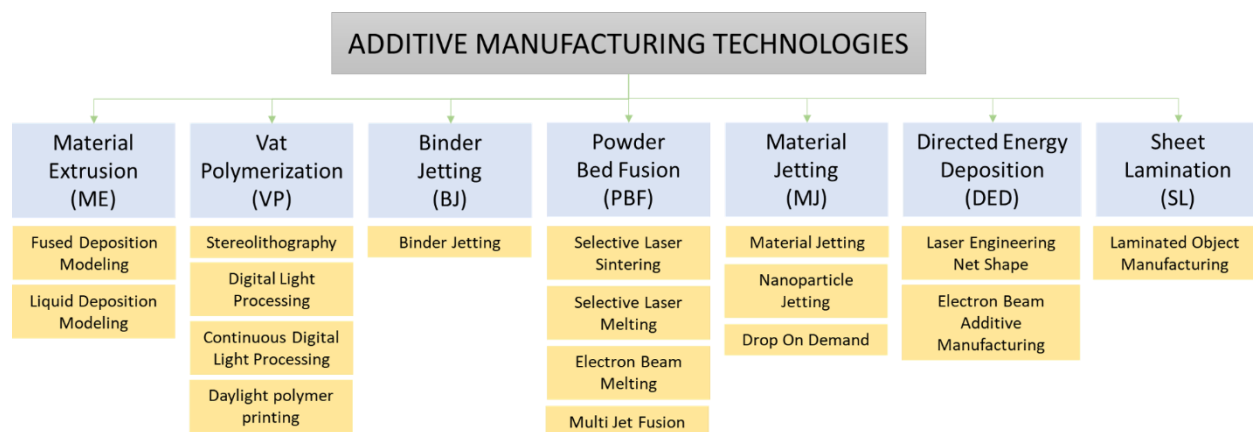
Figure 1.1 Categorization of Additive manufacturing technologies [3].

Material-based extrusion is a popular additive manufacturing approach. Additive manufacturing (AM) techniques are capable of meeting this need while also attaining zero waste by lowering the material-to-product ratio [4]. The ease of accomplishing rapid prototyping applications positions AM methodologies as an integral component of the sustainable manufacturing landscape [5, 6]. As a manufacturing concept, rapid prototyping (RP) refers to a collection of production processes used to quickly build a functioning component, element and or assembly using derived 2-D profiles from processed computer assisted design (CAD) data. The 2-D profiles are built in 2-D layers that are built on top of each other. The application of a layer-wise technique in production is at the heart of additive manufacturing. This approach is also applied in developing fuel cells [7].

1.1.1   Fused Deposition Modelling

Scott Crump invented and patented FDM as an additive manufacturing process. STRATASYS, Inc. owns the industrialised version of FDM [8]. **Figure 1.2** depicts FDM technology, which is effectively a G-code controlled vertical material extrusion process. FDM manufactures parts that are suitable for mechanical, chemical, and biological applications (end-use parts). **Figure 1.2** depicts the fundamental components of the FDM process. The fused deposition modelling process begins with the appropriate slicer software. The slicer software receives the 3-D CAD information for the part in the form of a stereolithography (STL) file.

Polymeric materials are usually employed in FDM. PLA is a accepted polymer employed in desktop printing [9]. Although the basic tolerances and accuracy of FDM printed materials are primarily determined by the printer's calibration and the complexity of the model. PLA is not as ductile as certain other thermoplastics, such as ABS, hence it is commonly used for rapid

prototyping where the form is vital and thus process parameters has a significant role during printing.
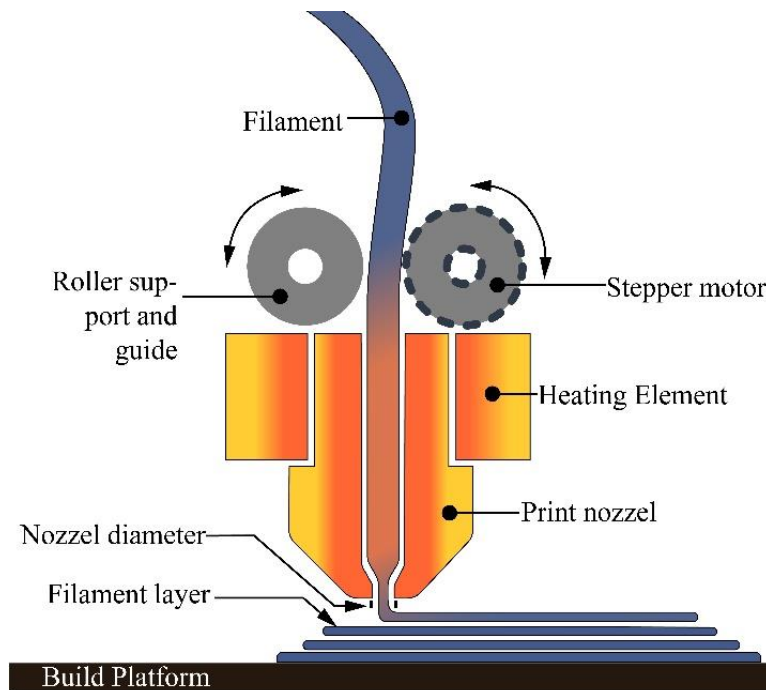
Figure 1.2 Basic components of material extrusion process.

To handle larger pieces and print at greater deposition rates, build volumes are raised. In 2014, Qingdao Unique Products Develop Co Ltd, a local manufacturer of 3-D printers in China, produced a printer with a build volume of 12 x 12 x 12 m for the purpose of building construction. The usage of light weight graphene glass fibre reinforced plastic as printing material is one of the new printer's major advantages. The printing material is also tough, corrosion-resistant, and eco-friendly. Builders Extreme 2000 3D, with a build space of 700*700*1820 mm with an integrated heated bed, two nozzles, and colour-mixing possibilities, is another example of a printer. The InnoFil Pro1 filament is made of reinforced PLA, making it suitable for engineering-grade 3D printing. The Delta Wasp 3MT 3D printer by Italian 3D printing pioneers WASP. Is able to 3D print concrete, clay and plastics a layer

resolution 0.5 mm and on a cylindrical build space of 100 x 100 cm. In addition, has the capability to act as a CNC mill. The Big Delta 3D printer, released in September 2015, prints clay funneled through a central nozzle.
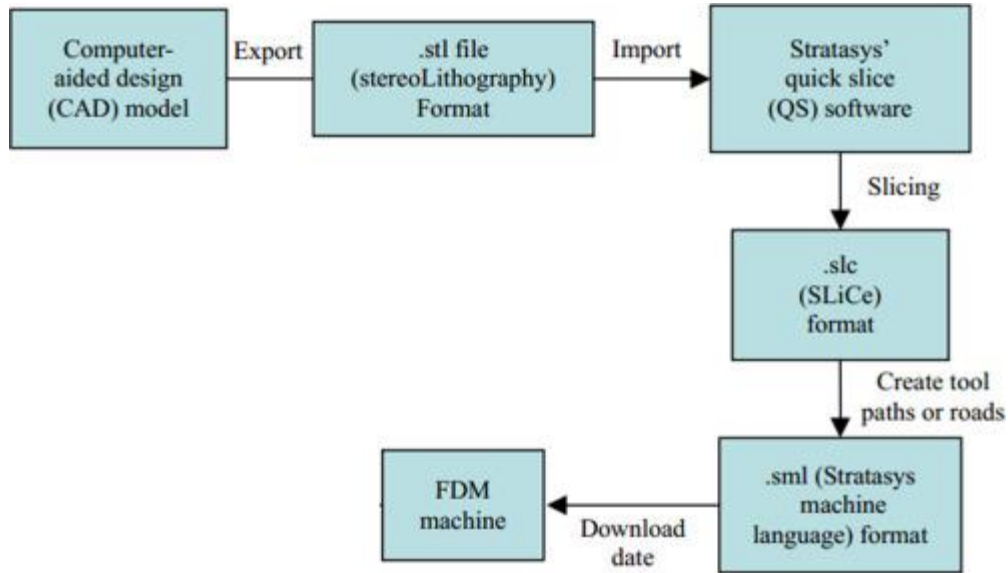
Figure 1.3 Basic procedure involved in FDM process *[10]*.

The UPrint SE series, with dimension-1200es series, Stratasys' Mojo, MakerBot's Replicator, 3D System's Cube and Fortus-250mc series are also examples of FDM printers. FDM machines have been developed by various manufacturers and the FDM process is performed by the numerous machine models. However, the basic steps of the process as shown in Fig. 1.3 is unchanged. Raising the material (polymer) till the glass transition point (temperature) is an essential phase in the FDM process [11]. Extrusion is more efficient at temperatures significantly greater than temperature at the material's glass transition. At these temperatures, the viscosity of the polymer decreases while its flow increases.
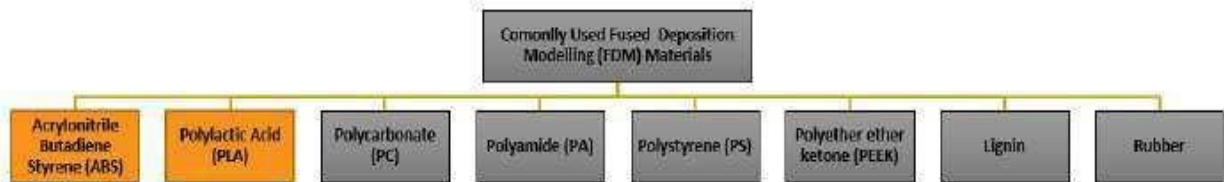
Figure 1.4 Materials commonly used in FDM.

1.1.2 Image Based Thermography

While modern additive manufacturing machines are substantially improved over previous versions, many of the same concerns highlighted by early researchers in the 1980s (temperature management issues, porosity, cracking, material supply issues) persist. This is largely attributable to a lack of in process monitoring and closed loop control algorithms used to manage machine operation [12]. Image-based thermography relies heavily on infrared imaging. The benefits of thermography include its non-invasive and relatively quick approach, as well as its capacity to process and present surface temperature distribution during FDM [13].

1.2 Research Rationale and Objectives

FDM Selecting the appropriate 3D printing material to manufacture them is also enhance the mechanical performance of the workpieces. The most often used polymeric materials in FDM techniques are acrylonitrile-butadiene-styrene (ABS) and polylactic acid (PLA). For certain applications, other materials such as composites and ceramic are also used. Many authors have characterized the mechanical behaviours of each material to confirm which materials are suitable in different cases [14]. For the estimation of these properties of materials different mechanical assessments are used such as bending tests [15], tensile tests [18–20] and fatigue tests [10, 21, 22].

Since AM have progressed so greatly, then there must be many challenges to be addressed, especially when refers to Replication Rapid Prototyping machines [22]. AM is typically utilised in small-scale applications and is built as an open-source device, allowing users to customise and modify production routines by changing different parameters to generate G-Code. Therefore, the use of the Fused Deposition Modelling technique in 3D printing is becoming popular, and its parametric optimization is even more crucial for the reduction of processing time and cost. There are different techniques used to optimize FDM process parameters, such as Taguchi's methodology, surface response methodology, etc [23, 24]. Also, in terms of convergence time, the precision of tests, and so on, they have obvious disadvantages. The key issue connected with the modern Taguchi approach, for example, it's inability to be used for the simplification of multi-objective test sets [25–27]. Hence, the process variables of FDM were attempted to be optimized with iterative algorithms [28]. The primary advantages of these algorithms are their versatility to be applied to/versatility with regards to application over any type of constrained or unconstrained problems. Global search, optimization, and generalization [25, 26] can be carried out by genetic algorithms (GAs). A number of parametric issues in production and manufacturing processes have also been solved by artificial neural networks (ANNs), such as the recognition and learning patterns in any data set and the improvement of recognition capability, predict, cluster, or model patterns [27, 28]. Here the feasibility of integration ANN modelling with GA optimization was implemented to predict optimum FDM parameter conditions. The development of an artificial neural network and genetic algorithm (ANN-GA), a method of modelling and optimization used to optimize a multi-objective problem, is defined in this research study. The effect of process parameters on Flexural strength 'E' and the 0.2% offset yield strength. Furthermore, a parametric study is also done.

LITERATURE REVIEW

With the increasing demand for higher quality, faster reproducibility, faster delivery, and mass customization, the introduction of additive manufacturing into the manufacturing sector provides relief to both ends of the Supply Chain, namely the producer and the end consumer. It was unthinkable a decade ago, but it is gradually becoming the norm in our society.

Figure 2.1 Contribution of AM in different Sectors

Additive Manufacturing is quickly becoming one of the most ground-breaking technological applications in the manufacturing industry. According to the Wohler's Report (2018), motor vehicles and aerospace, medical and dental, and business machines

and consumer products contributed 77.9 percent to the industrial adoption of additive manufacturing. In 2018, 3D printing metals saw the greatest growth of 42 percent.

2.1 Need for Additive manufacturing in industrial sector

By lowering delivery costs and shortening delivery lead times, additive manufacturing technology has the ability to alter the dynamics of traditional supply chain systems. Using AM technology, there can be on demand production of parts by the manufacturers, thus reducing the need and cost of maintaining spare parts inventory. With this technology, the user can make parts of practically any shape without the typical limitations like the manufacturability limitations. In addition, series of parts with individual changes can be made as simply as is the case of identical parts.
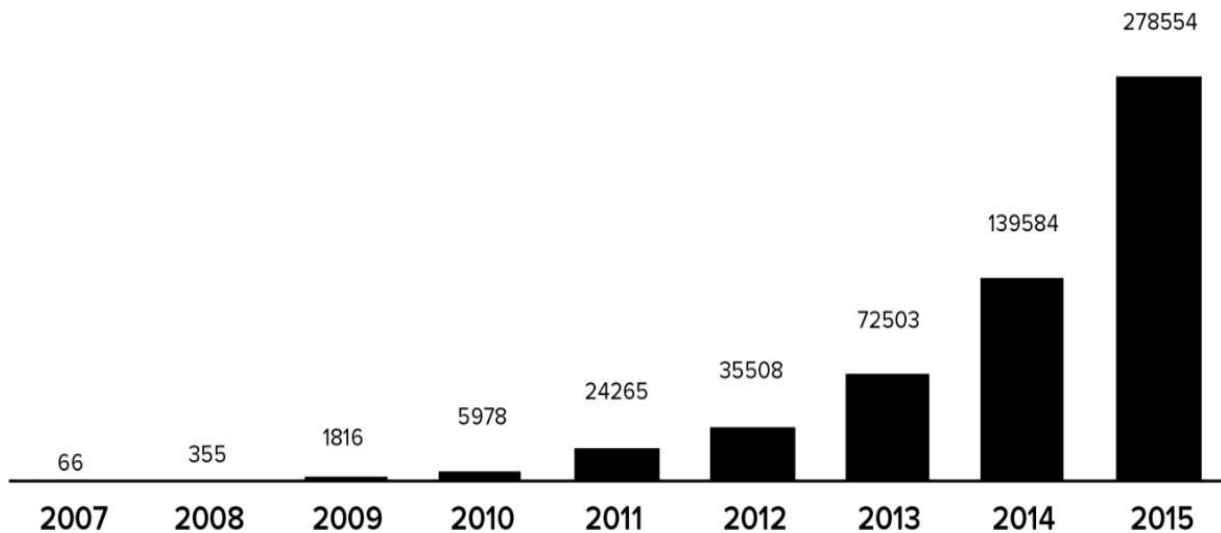
Figure 2.2 A graph showing the increasing trend in AM usage

Nexa3D creates ultra-fast 3D printers that can reduce printing cycles of precision functional parts from hours to minutes. ParaMatters designs and manufactures AM-ready, high-quality, lightweight parts for aerospace and automotive applications. UNYQ employs 3D printing to create novel mass-customized products that reinterpret

orthopaedic devices. Supercraft3D uses 3D printers to create medical models for use by surgeons, educational institutions, and diagnostic centres.

Figure 2.3 Benefits of using AM

Additive manufacturing is the process of producing parts by layering raw materials one by one in order to obtain a part with the required digital design fed into the software.

Because 3D printing machines are used in the process, it is also known as 3D printing. Rapid prototyping is a set of methods for quickly transforming a design/model of a part or parts into a scale model using 3D computerised design. The three terms are used interchangeably.

Additive Manufacturing is a disruptive innovation and is being adopted by the Industry and research by the academician. Extensive developments are taking place in making this technological development useable for the Industry. Presently industry is using this extensively in the product design supply chain. The adoption of AM in the industry is still very limited, and there has not been much on research about the impact additive manufacturing in production systems - enabling the demand driven supply chain.

2.2 Process of the 3D Printing

The FDM process is an additive manufacturing technique based on material extrusion. The basic components are presented in **Figure 2.4** from [33]. The operation entails layering polymeric or metal filament that has been unwound from a spool along the X, Y-axis. Following the completion of each layer, the extruder head moves upwards (positive Z orientation) for the next layer.
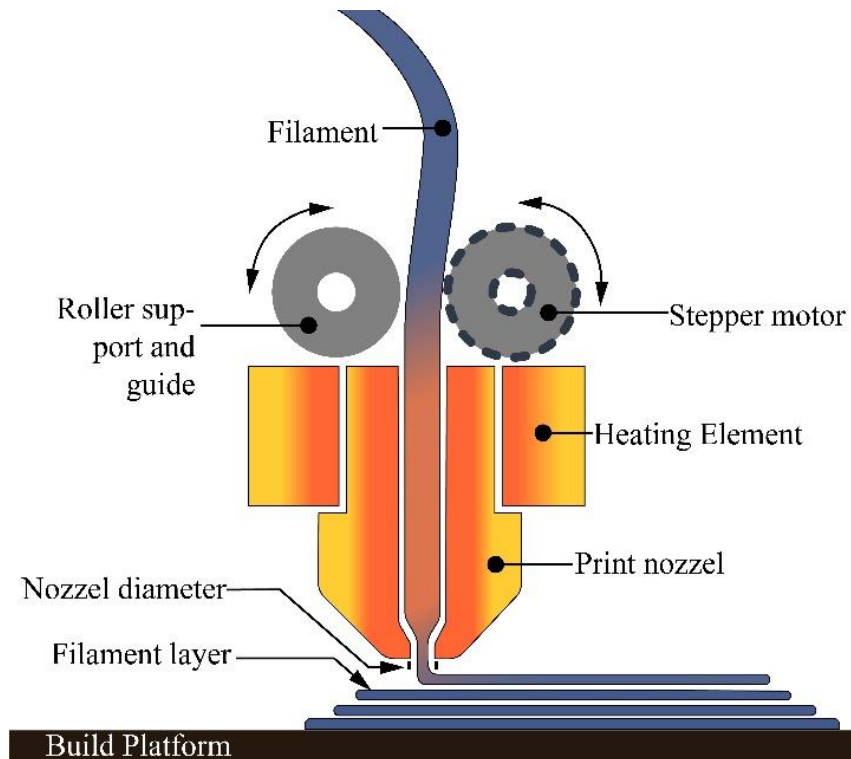
Figure 2.4 Schematic view of the fused deposition modelling process components.

Because the nozzle incorporates resistive heaters that hold the plastic at a temperature just above its melting point, allowing it to flow freely and build the layer, the produced material is often made available in filament form. As the plastic bonds to the layer below, it instantly hardens. The platform lowers as soon as the layer is completed, and the extrusion nozzle deposits another layer. The visibility of the printing layers is a distinguishing feature of FDM printing.

FDM represents one of the most common techniques for proto-typing in AM [34]. It is one of the additive manufacturing technologies that has dramatically changed the printing and manufacturing industries. It broke the printing industry's 2D printing limits, allowing anyone to easily bring their 3-dimensional virtual world creations to reality. The manufacturing industry's creation of items is no longer limited to the conventional system of using manual

labour and distinct machinery for different portions. FDM technology, on the other hand, has limits. The materials that can be copied, difficulty in 3D printing highly detailed products, and challenges with end product quality are three of these significant limits. As a result, there has always been a need for development, especially in these three areas. Hundreds of FDM printer manufacturers exist today, some of which produce open-source FDM printers. Most of these manufacturers work hard to suit society's current demands. FDM research is classified into three categories: innovative applications, materials, and system enhancements. The great majority of system improvements are software-based, such as tool path creation and slicing algorithms and part orientation optimization.

2.3 Thermomechanical Aspects of Fused Deposition Modelling

The temperature of the material is raised to its glass transition temperature during the extrusion process (this differs from the material's melting point). The glass transition temperature denotes the temperature at which the amorphous phase begins. This differs from the melting point (where crystalline phase separates and starts to flow). Temperature is higher than room temperature for plastics. [35]. Fig. 2.5 and Fig 2.6 from shows a drop in elastic modulus as temperature increases. As the temperature rises, the polymer transitions from a glassy state to a leathery state, then to a rubbery state, and finally to a liquid flow.
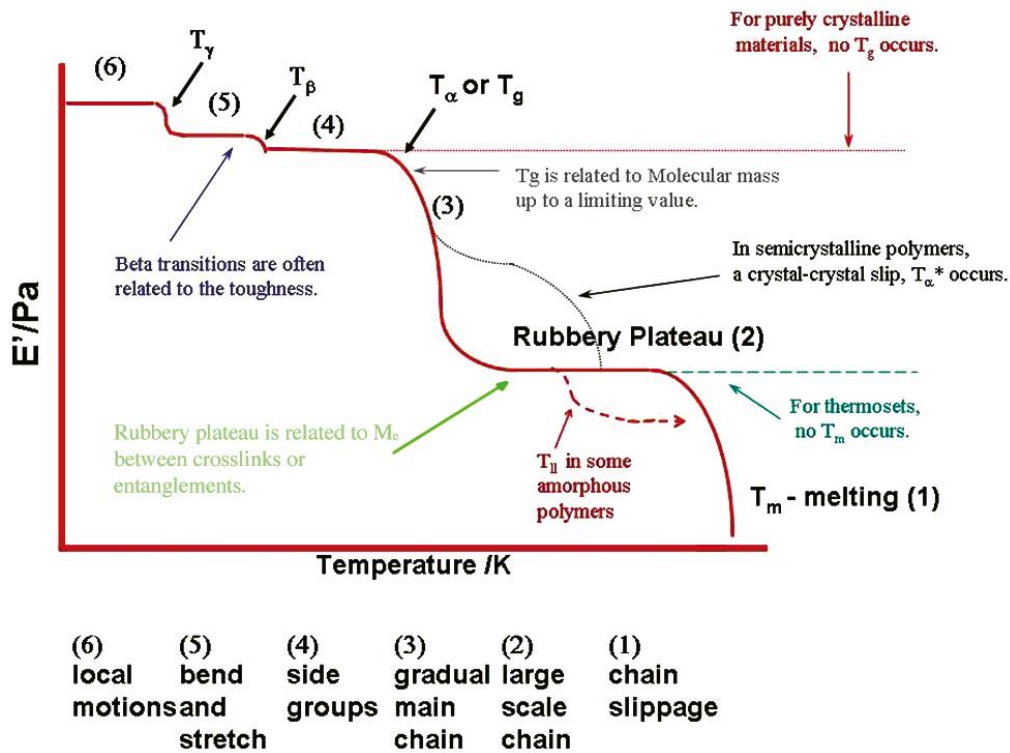
Figure 2.5 Modulus values change with temperature and transitions in materials can be seen as changes in the E' or tan delta curves.
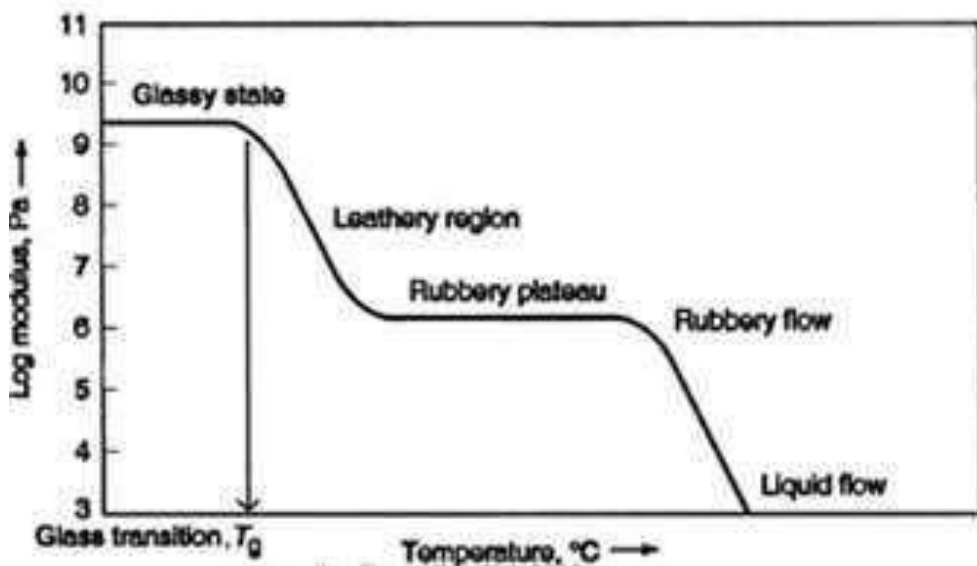
Figure 2.6 Plot showing the influence of temperature on elastic modulus of plastics.

FDM fabricated parts also show anisotropic material behaviour [36]–[38]. This has been observed through the strength analysis effect of print orientation and other spatial

13

parameters such as raster path on FDM printed parts. The tensile and yield strength results show a significant anisotropic effect [39]–[42].

2.4 Potential Defects in Fused Deposition Modelling

Defects generally arise from either the print material characteristics (which dependent upon its mechanical and rheological properties) or from the fused deposition processes [43]. Defects can occur in regions of enhanced stress concentration [44]. Sharp features that amplify mechanical stress have a negative impact on the ultimate mechanical properties. As a result of the staircase and slicer conversion effect, surface flaws emerge (which produces polygonal finite elements). Surface faults can also appear as burrs in the support structure, furrowed top surface, and start/end problems.

The slice manufacturing method is primarily responsible for the staircase effect; it can be corrected by adjusting the layer height and processing strategy. The chordal effect, on the other hand, is caused by 'stl' files, which approximate surfaces as a web of triangles and are commonly used by many RP methods. Although choosing a different surface modelling format will be effective, a short-term solution will be to offset the part positively and complete with a post-process finishing [45].

Internal defects in polymer and green ceramic parts can be caused by a combination of hardware and software constraints as well as material properties. Voids in the surrounding areas of the borders caused by poor filling can result in insufficient material flow filling up the intersections, resulting in a void. This challenge can however be corrected by allocating a negative offset to the perimeter and expanding the flow rate at the points of intersection [43].

Warping and curling defects, as shown in Fig. 2.7, manifest themselves as the printed part curving or bending upwards from the build plate or platform. The build layers cool as

they are deposited; however, previously deposited layers have already cooled and contracted.
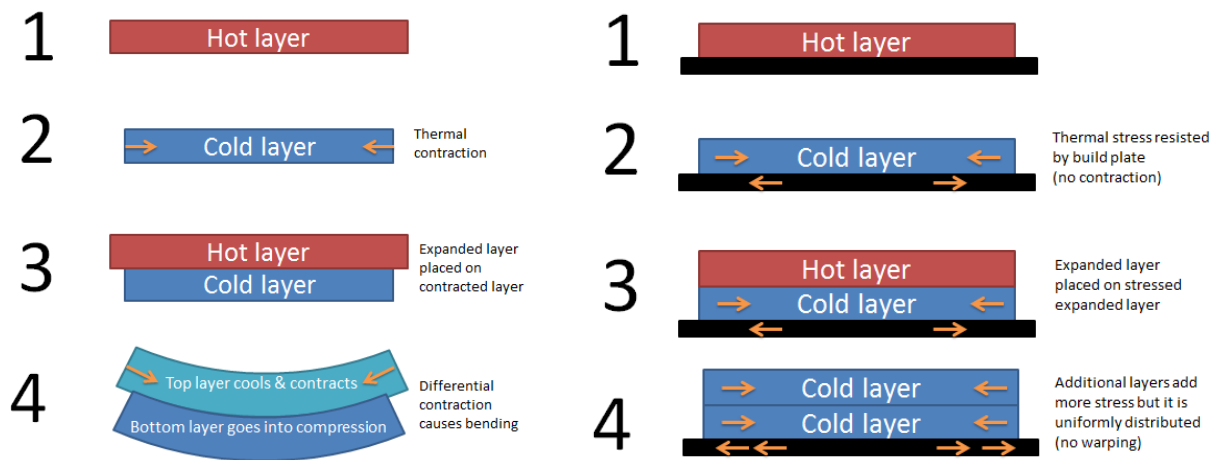
Figure 2.7 Cooling of build layers and part contraction in FDM process.

As a result, the top layer contracts in relation to the bottom layer. New layers have a higher temperature than the previous one, resulting in a thermal gradient between the layers and the resulting thermal stresses. Warping occurs as a result of the part cooling and contracting. Furthermore, when the thermal stresses are greater than bonding between the base layer and the build plate this leads to the part edge curling upwards [46].

To facilitate a better printing process, the build plate temperature is raised prior to material deposition during printing to avoid warping. Furthermore, the build plate temperature is kept slightly below the point at which the material begins to solidify (glass transition temperature). Thus, ensuring that, the base of the build part stays flat and adhered to the build plate [47].

Elephants foot defect occurs when the first layer of a structure is unable to support the weight of subsequent layers. As a result, the base of the part swells outwards.

The presence of excess melted material in the extruder nozzle is referred to as a string defect. As a result, unwanted thin strips of print material are produced. This

causes the print material to dribble. Printer manufacturers have integrated retraction capabilities into the printer nozzle to prevent strings

2.5   State of the Art in Fused Deposition Modelling

Shortening build time and improving the surface accuracy especially for complex product models is an important interest in research in RP [48]–[50]. The slicing process is also susceptible to the stair-case effect, leading to poor surface quality of end-products [50], [51]. The adaptive tool path generation method is a viable solution to these concerns [52]. The trajectory of the nozzle (print head) during the manufacturing process is referred to as the tool path in FDM to fill the interior of each layer. There are two main tool path trajectories for FDM processes: contour parallel path and orientation parallel path [53] as shown in Fig. 2.8 from [52].

Jin et al. [52] proposed an approach which covers both surface accuracy and fabrication efficiency. The proposed method is divided into three steps. For the following tool path generation, an adaptive slicing method that takes into account both surface quality and building time is proposed first. Adaptive slicing can reduce the staircase effect by adjusting layer thickness based on the geometric properties of models.

Second, a hybrid tool path strategy was introduced to improve the accuracy of the boundary contours and reduce the time required for interior filling. This step is an adaptive process that determines the best proportional relationship between the two types of tool paths: contour parallel path and direction parallel path, based on the specific fabrication requirements.

Unfilled areas and unstable speed result from abrupt changes in tool path orientation. Tool path adjustment reduces errors and helps to improve fabrication quality.
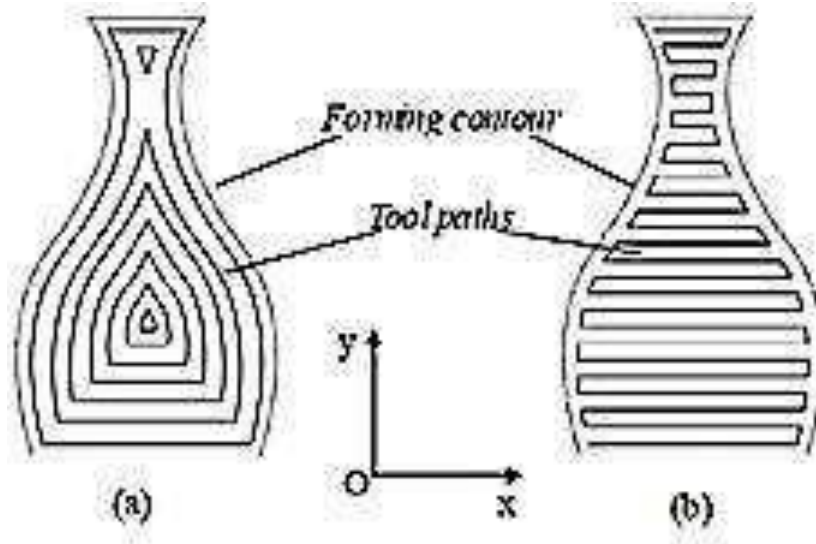
Figure 2.8 Cooling of build layers and part contraction in FDM process.

The tool path adjustment allows for a better balance of fabrication quality and building time. This balance was achieved by selecting the nozzle speed, the number of contour parallel tool paths, and the orientation of parallel tool paths. The parameters are chosen based on the accuracy required and the geometrical information of the model. 3D Printer farms are the most recent in small manufacturing technology and an example of an improved software-based system. It is the configuration of multiple printers in a cluster to run and monitor the printers using common software. Products can be produced at higher speeds and brought to market faster by utilising multiple printers set up in an array. The initial investment is less than that of purchasing a single industrial 3D printer, and the array can be scaled up more economically as needed. The Stratasys Fortus 380 is an example of an FDM printer farm. It has a maximum print size of 355 x 305 x 305 mm and can print in 7 materials including ABS, ASA, PC and Nylon. According to founder Rene Gurka, founder of BigRep, the true future of 3D printing is in 3D printing farms, where numerous large-scale models work in tandem and are managed by a single system. As FDM extruder technology evolved, material deposition techniques such as adaptive filament deposition

(AFD) and planar layer deposition (PLD) were developed for freeform metal and ceramic manufacturing. AFD controls the volumetric flow rate of liquids through the extrusion orifice by using a conical spindle inside a deposition head. The liquid jet is cooled by the ambient air temperature after leaving the orifice and becomes a filament. Retracting the spindle away from the orifice allows for higher flow rates, resulting in a larger filament.

Various polymeric materials have been explored for application in FDM, however commercial FDM machines mostly use acrylonitrile butadiene styrene (ABS) and polylactic acid (PLA) [20].

While there are different types of materials that can be used in AM, the material properties are typically not as strong as their conventionally manufactured counterparts due to the anisotropy caused by the layer-by-layer [54]. Recent research has shown the viability of composite materials such as metal matrix composites, ceramic composites, natural fibre-reinforced composites and polymer matrix composites [55]. Researchers at Rutgers University in the United States have developed fused deposition of ceramics (FDC) [10]. Currently, the most frequent FDM filaments for printing components are PLA, ABS, and Nylon, while PVA and HIPS are the most used support filaments because to their dissolvability. TPE or TPU (Thermoplastic polyurethane) filaments print parts with much higher elasticity than ABS and PLA. Carbon fibre, metal powder, or wood fibres with PLA, Nylon, or ABS are examples of composite filaments. Nylon has the highest strength and flexibility of the three most common filaments, followed by PLA, which has a medium strength and the least flexibility. Finally, ABS has the lowest strength while being more flexible than PLA. ABS has the advantage of being dissolvable in acetone which gives the ability to chemically treat its surface for better finishing [60].

2.6 Research in Monitoring Fused Deposition Modelling Process

The observation of the interior workings of the 3D printer during the fusion process stage is referred to as additive manufacturing process monitoring. Process monitoring also encompasses the observation of the printing process parameters [56]. An understanding of what takes place during this stage will lead to the development of a quality control system which would aid in industrial additive manufacturing [12]. This is critical in the biomedical, aerospace and defence industries, also would improve manufacturing time and enhance mass production of customized parts. In their study, [57] used ultrasonic excitation as a means of detecting filament bonding failures introduced by manipulating the print bed temperature during the fused deposition modelling build process. The work demonstrated the capability of correcting these filament bonding failures by introducing a correction mechanism through tunable control of another printer process parameter. The results demonstrated progress toward fully closed loop control for fused deposition modelling processes by demonstrating the detection and correction of filament bonding failures in situ.

Nozzle clogging in FDM printer extruders leads to process errors and subsequent print failure. Current FDM machines have limited techniques to monitor process conditions to minimize process errors such as nozzle clogging, [58] presented a physics-based dynamic model suitable for monitoring nozzle clogging in FDM. The method involved simulating nozzle clogging with nozzles ranging in diameter from 0.5 to 0.2 mm and change intervals of 0.1 mm. Experiments were conducted by measuring the vibration of the liquefier block mount during material extrusion. The results showed that the amplitude of the liquefier block mount transverse vibration increases non-linearly as the nozzle blockage progresses. As a result, there are compelling arguments for incorporating sensors to detect the onset of nozzle clogging as a viable solution. Despite ongoing research to improve current AM products, issues such as

porosity, cracking, thermal management issues, and material supply issues persist. This is attributable to the inadequacy of integrated systems to study the on-going fabrication, and closed loop control algorithms for machine operation oversight [12]. Because of the aforementioned scarcity, manufacturers adjust process parameters based on heuristics and previous fabrication runs, yielding limited improvement in part quality and necessitating numerous builds runs for convergence. While some process monitoring methods can be applied to all additive manufacturing techniques, others are specific to a specific 3D printing type and can only be adapted to it.

The typical machine condition monitoring sequence includes fabrication parameter choice protocols, perception and data retrieval, data conversion handling and attribute elicitation, intellective judgment and response [59]. Data-driven models utilize historical data only to build analytical models for product property or failure predictions [60]–[63].

In a study on process monitoring, [59] employed acoustic emission (AE) technique for in-situ monitoring of FDM machine conditions. The method identified and classified machine normal and abnormal states. The normal states of the machine were determined to be material loading, normal extruding, and idle. Print material run-out, extruder semi-blocked with chatter and uneven extrusion due to heater breakdown, low-quality filament, extruder wear, or working environment contamination, and total blockage without extrusion were all classified as abnormal machine states. The time-domain characteristics of AE hits were used as indicators. The FDM printer states monitored during the fabrication process are shown in Fig. 2.9 as an overview of the AE approach. Temperature fluctuations, distribution and the influence of fabrication process thermal loads developed during the building process also affect the FDM product quality [64], [65]. Also [66] carried out numerical study on temperature distribution during the FDM process.

Embedded thermal sensors provided real-time and in-situ monitoring during the fabrication of multi-layered thin plates.
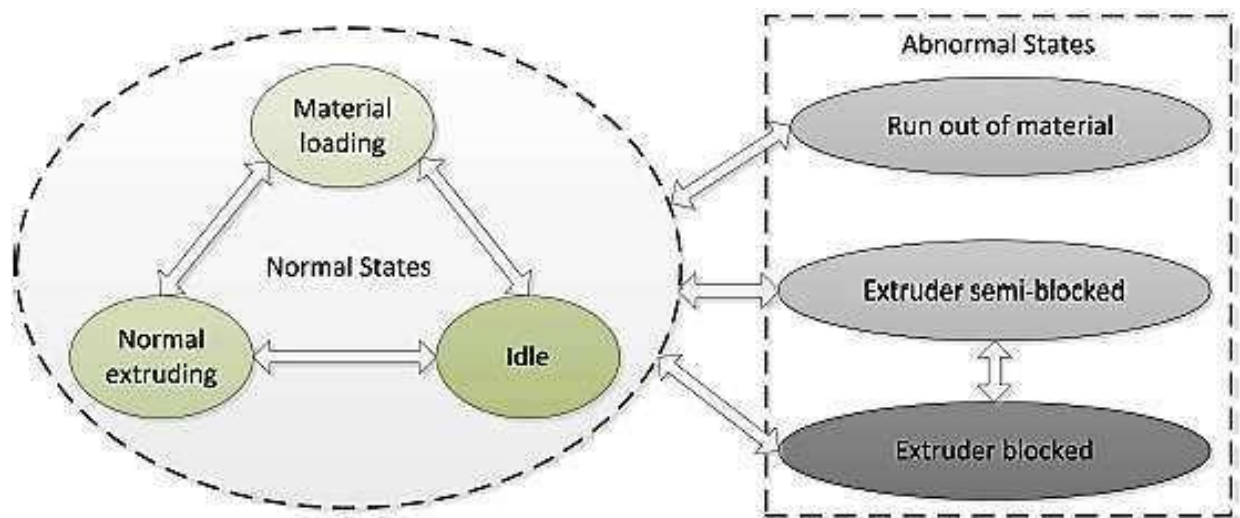
Figure 2.9 Machine conditions during FDM fabrication process.

EXPERIMENTAL INVESTIGATION

3.1 Materials and methods

3.1.1 Materials used

Acrylonitrile Butadiene Styrene (ABS) were used to manufacture specimens for the study to obtain the performance of 3D printing by FDM technique. This material ABS (grey) are manufactured and provided by the Shenzhen Creality 3D Technology Co., Ltd. The characteristics of the materials according to the manufacturer are listed below in **Table 1**.

Table 1 Properties of materials used for 3D printing (FDM)

Characteristic	ABS
Filament diameter (mm)	1.75±0.03 mm
Material density (g/cm^3)	1.04
Tensile Yield Strength (MPa)	39
Elongation at break (%)	20
Flexural Strength (MPa)	60
Flexural modulus (MPa)	1,900
Tensile modulus (MPa)	Not provided
Print temperature (°C)	210 –240
Hot Pad (°C)	80 – 105

3.1.2 Specimens

The specimens were manufactured according to the guidelines included in the ASTM D7264 standard, which also describes how the three-point bending tests must be conducted. They have

a prismatic shape and dimensions of 80x13x4 mm as shown in **Figure 3.1**. They were printed on a CREALITY ENDER 3V2 printer from the Shenzhen Creality 3D Technology Co., Ltd. To have stabilize the manufacturing conditions, all 27 specimens were manufactured at the same environment.
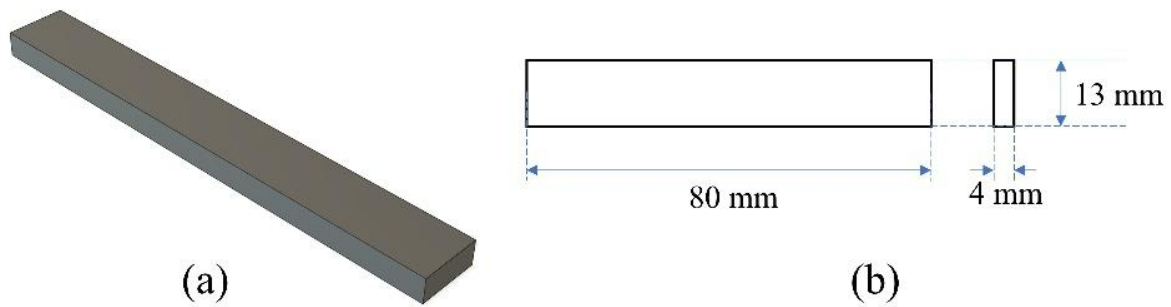
Figure 3.1 (a) Prismatic specimen (b) Specimen's dimension

3.2 Mechanical testing

The prismatic specimens were 3D printed and then it was subjected to three-point bending tests according to ASTM D7264 standard. This method consists of performing a test with a specimen (prismatic bar) rest on two supports and is loaded by means of a loading nose midway between the supports. This method has proved to deliver reliable results in other parts obtained by AM techniques [67]. In this study Flexural strength 'E' in GPa, and the 0.2% offset yield strength (or 0.2% proof stress, $R_{P0.2}$) in MPa are taken as output parameter in the experiments.

3.2.1 Flexural strength and 0.2% offset yield strength Testing

By using flexural testing, we can determine the behaviour and mechanical properties of 3D Printed beams. And this flexural property of 3D printed beams was analysed by following ASTM D7264. Then to improve the 3D printed beam flexural capacity and overall strength, design enhancements were done. Bending of 3D printed beam using three-point flexure testing can be achieved by applying a point load at the centre of the 3D printed beam inducing bending moments (BM) throughout the 3D printed beam, with highest BM at the centre of the 3D

printing beam. From the three-point flexural test, force-displacement data usually obtained. After that, from stress-strain diagram the flexural properties of the 3D printed beam can be determine, which would also lead to flexural modulus, shear strength and other important mechanical properties. Flexural stress is controlled by moment of inertia, the bending moment and the distance to the neutral axis. Also, a 0.2 % offset yield strength (0.2% OYS, 0.2% proof stress, RP0.2) that is an amount of stress which will get in 0.2% of plastic strain. This yield strength is most often used by design engineers and material suppliers. For a different specified parameter set, there will be a different yield strength related with that strain level.

4.3 Experimental design

This study took into consideration the influence of six different variables: nozzle diameter, layer height, fill density, printing velocity, raster orientation and infill pattern. For each parameter, three levels were defined, as can be observed in **Table 2**.

Table 2 Factors and levels used in the study

Factor	Level 1	Level 2	Level 3
Nozzle diameter (mm)	0.3	0.4	0.6
Layer height (mm)	0.1	0.2	0.3
Infill density (%)	25	50	75
Printing velocity (mm/s)	20	30	40
Orientation	X-axis (0°)	45° with X-axis	Y-axis (90°)
Infill pattern	Rectilinear	Linear	Honeycomb

To perform the minimum number of experiments, a Taguchi L27 DOE was applied to combine the factors given in **Table 3**. This array allows the extraction of results regarding the influence of all factors as well as three interactions between the nozzle diameter, layer height, fill density, printing velocity, raster orientation and infill pattern. 'Infill patterns' viz rectilinear, linear and

honeycomb are set as three different individual factors. These three factors are coded using One-Hot encoding method between '1' to '0' value, '1' is for full weightage and '0' is for factor's zero effect on process. Each row of the array describes the combination of factors to obtain each type of specimen. For each of them, three identical specimens were tested for each of them, to confirm the repeatability of results. Therefore, the results of 81 trials were tested and evaluated.

The slicing software ULTIMAKER CURA used to obtain the G-CODE to manufacture the specimens that offers the possibility of changing many other variables, that were kept constant in this case. For this reason, there are a series of parameters can be controlled. The reader can refer to the ULTIMAKER CURA user manual regarding the additional parameters in it. It is worth mentioning that, as there are no standards regulating how additive manufactured specimens should be tested. it was decided that 0.8 mm would be the perimeter width. The Schematic of 3D printing optimising process is given in **Figure 3.2**.
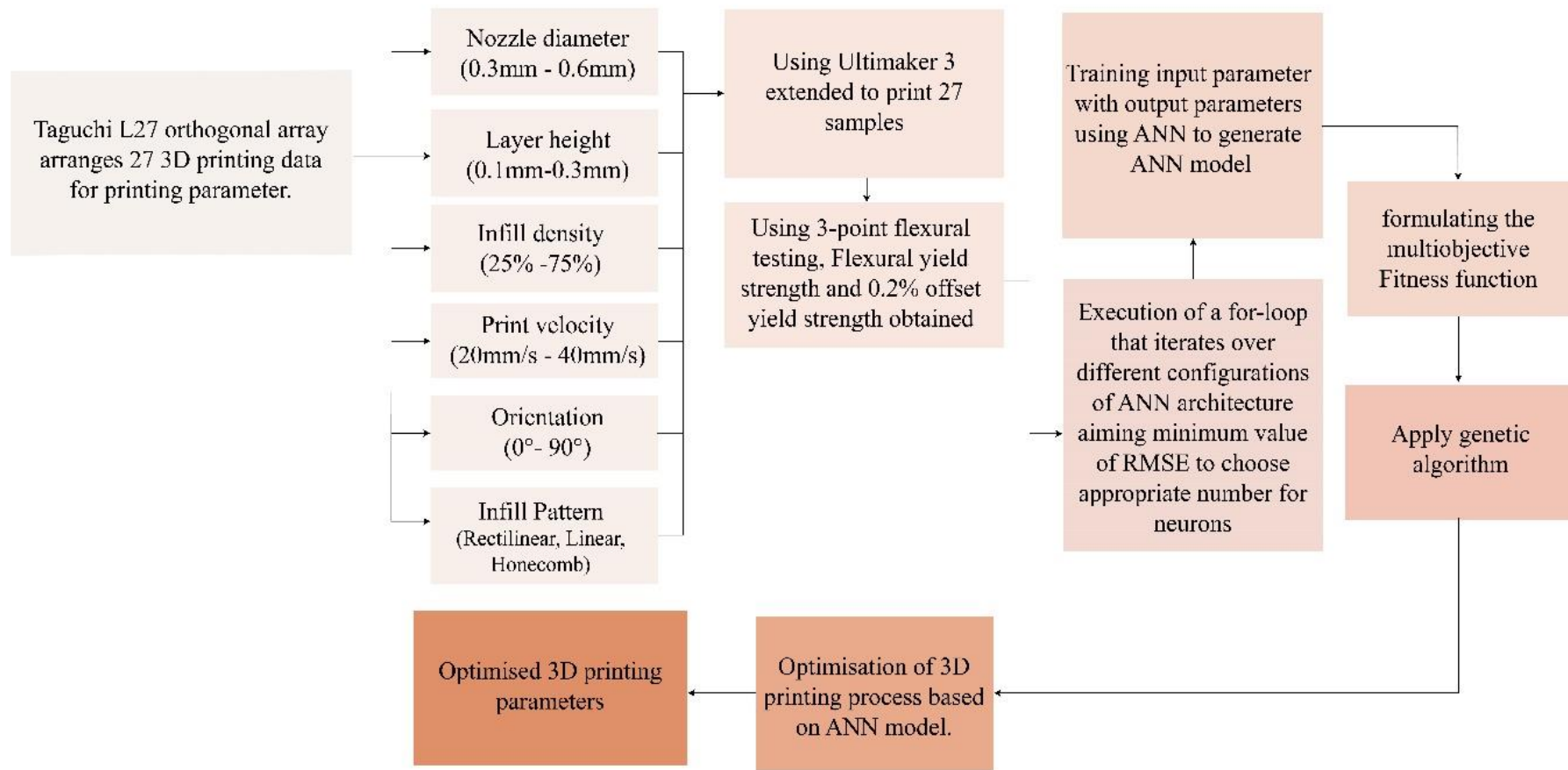
Figure 3.2 Schematic of 3D printing optimising process

Table 3 Experimental design represented by an L27 Taguchi orthogonal array

Run	Nozzle diameter (x₁) (mm)	Layer height (x₂) (mm)	Fill density (x₃) (%)	Printing velocity (x₄) (mm/s)	Orientation (x₅)	Infill pattern			Experimental		ANN Predicted		Absolute error %	
						Rectilinear (x₆)	Linear (x₇)	Honeycomb (x₈)	E (GPa)	$R_{P0.2}$ (MPa)	ANN Predicted E (GPa)	ANN Predicted $R_{P0.2}$ (MPa)	E (GPa)	$R_{P0.2}$ (MPa)
1	0.3	0.1	25	20	0	1	0	0	2.236	45.99	2.2360	45.9895	0.00	0.00
2	0.3	0.1	50	30	90	0	1	0	2.495	51.95	2.4733	51.9498	0.87	0.00
3	0.3	0.1	75	40	45	0	0	1	2.251	45.37	2.2617	45.3700	0.47	0.00
4	0.3	0.2	25	30	90	1	0	0	2.13	44.85	2.1300	44.8499	0.00	0.00
5	0.3	0.2	50	40	45	0	1	0	2.084	41.77	2.0945	41.7702	0.50	0.00
6	0.3	0.2	75	20	0	0	0	1	2.225	49.05	2.2250	49.0465	0.00	0.01
7	0.3	0.3	25	40	45	1	0	0	1.182	9.41	1.1820	9.4108	0.00	0.01
8	0.3	0.3	50	20	0	0	1	0	1.888	15.18	1.8880	15.0810	0.00	0.65
9	0.3	0.3	75	30	90	0	0	1	1.908	44.02	1.9088	44.0947	0.04	0.17
10	0.4	0.1	25	30	45	0	1	0	1.889	38.79	1.8890	38.7901	0.00	0.00
11	0.4	0.1	50	40	0	0	0	1	2.217	43.97	2.2246	43.9698	0.34	0.00
12	0.4	0.1	75	20	90	1	0	0	2.557	54.26	2.5570	54.4588	0.00	0.37
13	0.4	0.2	25	40	0	0	1	0	2.191	46.79	2.1910	46.7900	0.00	0.00
14	0.4	0.2	50	20	90	0	0	1	2.22	47.95	2.2200	47.9488	0.00	0.00

15	0.4	0.2	75	30	45	1	0	0	2.189	48.58	2.1890	48.5800	0.00	0.00
16	0.4	0.3	25	20	90	0	1	0	2.05	42.72	2.0500	42.5610	0.00	0.37
17	0.4	0.3	50	30	45	0	0	1	1.978	40.79	1.9780	40.6983	0.00	0.22
18	0.4	0.3	75	40	0	1	0	0	1.85	40.87	1.8500	40.8701	0.00	0.00
19	0.6	0.1	25	40	90	0	0	1	2.474	53.92	2.4740	53.9199	0.00	0.00
20	0.6	0.1	50	20	45	1	0	0	2.359	49.94	2.3457	49.9400	0.56	0.00
21	0.6	0.1	75	30	0	0	1	0	2.004	47.54	1.9010	47.5401	5.14	0.00
22	0.6	0.2	25	20	45	0	0	1	2.175	46.35	2.1750	46.3494	0.00	0.00
23	0.6	0.2	50	30	0	1	0	0	2.007	46.6	2.0070	46.4842	0.00	0.25
24	0.6	0.2	75	40	90	0	1	0	2.538	51.86	2.5380	51.8599	0.00	0.00
25	0.6	0.3	25	30	0	0	0	1	2.058	47.42	2.0580	47.4197	0.00	0.00
26	0.6	0.3	50	40	90	1	0	0	2.475	48.87	2.4750	49.4814	0.00	1.25
27	0.6	0.3	75	20	45	0	1	0	1.973	46.88	2.0554	46.8780	4.18	0.00

RESULTS AND DISCUSSION

4.1 Modelling and Optimisation

4.1.1 Artificial neural network

The Flexural strength 'E' in GPa, and the 0.2% offset yield strength (or 0.2% proof stress, $R_{P0.2}$) in MPa are modelled using the artificial neural network. The ANNs are individually developed for the modelling of the Flexural strength, and $R_{P0.2}$.

In this work, modelling for the 3D-Printing process using ANN architecture with a backpropagation algorithm was used precisely its output concerning input parameters. Modelling the ANN works in stages: training, testing, and validation [23–25]. The program codes were written for that purpose in MATLAB R2017a software. Experimental data was trained in the ANN architecture, which is shown in **Table 4**. The neural network contains three different layers of neurons, out of which the first layer includes neurons corresponding to input parameters [70]. The input layer contains '8' neurons synonymous to each of the input variables, where it can be noted that categorical factor i.e., 'Infill patterns' viz rectilinear, linear and honeycomb are set as three different individual factors. These three factors are coded between '1' to '0' value, '1' is for full weightage and '0' is for factor's zero effect on process. The 2nd layer is called the hidden layer. For the determination of the number of hidden layers and the number of neurons in each of them for multilayer perceptron, various hyperparameter tuning techniques may be used, ranging from sheer experimentation, referring to existing models for inspiration as well as optimization using algorithms such as Bayesian Algorithm [71]. Number of hidden layers were chosen '2'. The configurations of neurons with the lowest RMSE value for 'E' and $R_{P0.2}$ can be seen in **Figure 4.1**and **Figure 4.2** .
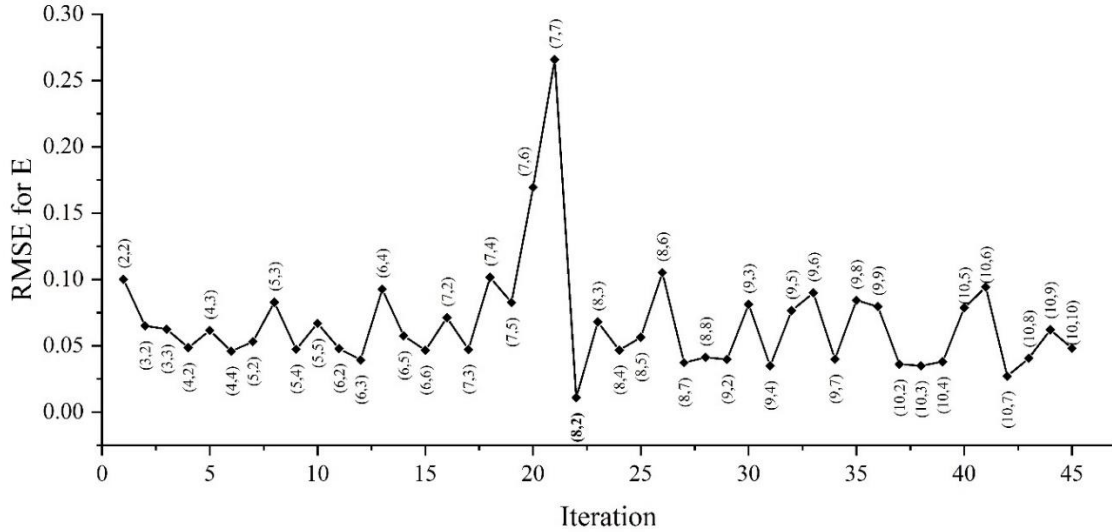
Figure 4.1 Configuration of neurons with the lowest RMSE value for 'E'.
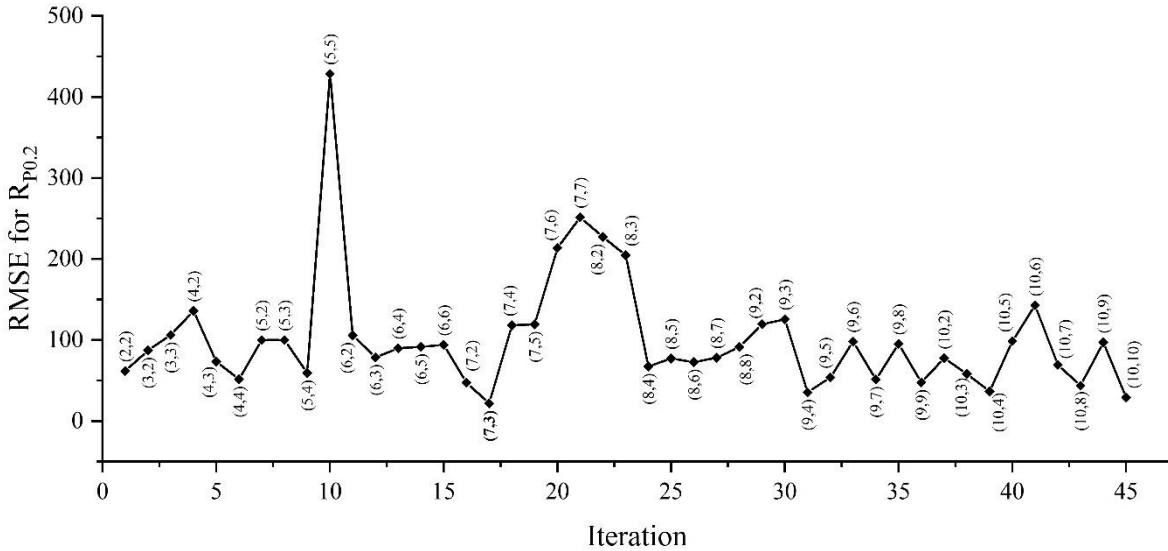
Figure 4.2 Configuration of neurons with the lowest RMSE value for $R_{P0.2}$

The configuration with the lowest RMSE value was taken to be the most suitable for this case and the final ANN was modelled based on this. Now, network has 8-2, and 7-2 neurons, respectively, for (E) and ($R_{P0.2}$) as shown in Table 4. The 3rd layer has '1' neuron corresponding to each output value. For the present data outputs, the "trainlm", Levenberg-Marquardt training method was used for quick supervised learning is easy, safe, and computationally less expensive because of its adoptive learning and no-line search technique [72]. The transfer functions selected for the hidden and output layers were Log-sigmoid and Tan-sigmoid,

30

respectively, which were calculated as given by Equation (1) and Equation (2) [73], [74]. For the training, testing and validation of ANN, 70%, 15%, and 15% data are used, respectively. Mean square error algorithm was used for performance of the training.

$$tansig\ (n) = \frac{2}{(1+e^{-2n})} - 1 \qquad (1)$$

$$logsig\ (n) = \frac{1}{(1+e^{-n})} \qquad (2)$$

Where n is input for the function.

$$Percentage\ error = \frac{(Experimental\ value - ANN\ predicted\ value) \times 100}{Experimental\ value} \qquad (3)$$
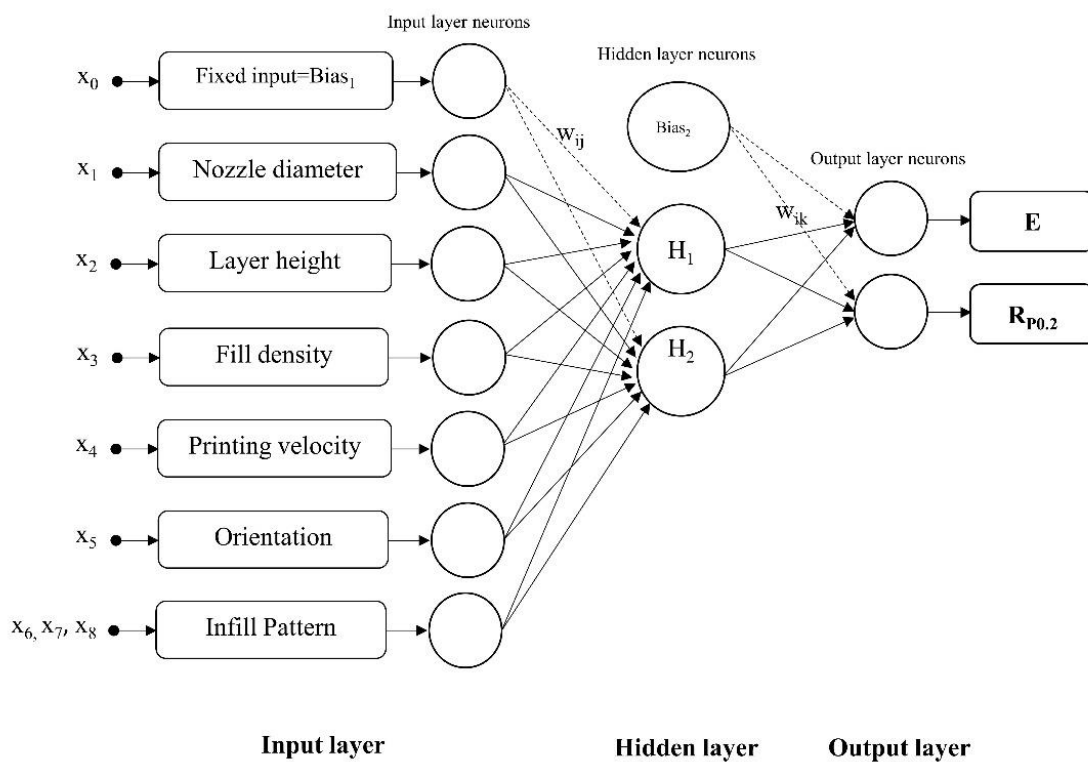
Figure 4.3 ANN architecture

Table 4 ANN architecture for input to output modelling

Input	Output	ANN architecture
$x_1, x_2, x_3, x_4, x_5, x_6, x_7, x_8$	Flexural strength 'E'	8-8-2-1
$x_1, x_2, x_3, x_4, x_5, x_6, x_7, x_8$	0.2% offset yield strength '$R_{P0.2}$'	8-7-3-1

31

The trained ANN performance for Flexural strength has been shown in Fig. 4.4, which tells the rationally good performance of trained ANN because the validation and test curves are on line, error histogram also confirms this fact in Fig. 4.7.

It cannot be ignored that the best validation performance has attained zero epoch with the value of $6.9244*10^{-14}$, where the training persists until the 3rd epoch, Fig. 4.6, shows best validation performance. Fig. 4.8., shows the training state of ANN, where the gradient coefficient's final value is $1.4206*10^{-9}$, approximately zero at the 3rd epoch. Also, a diminishing value of gradient can be seen with the increase of epochs number.
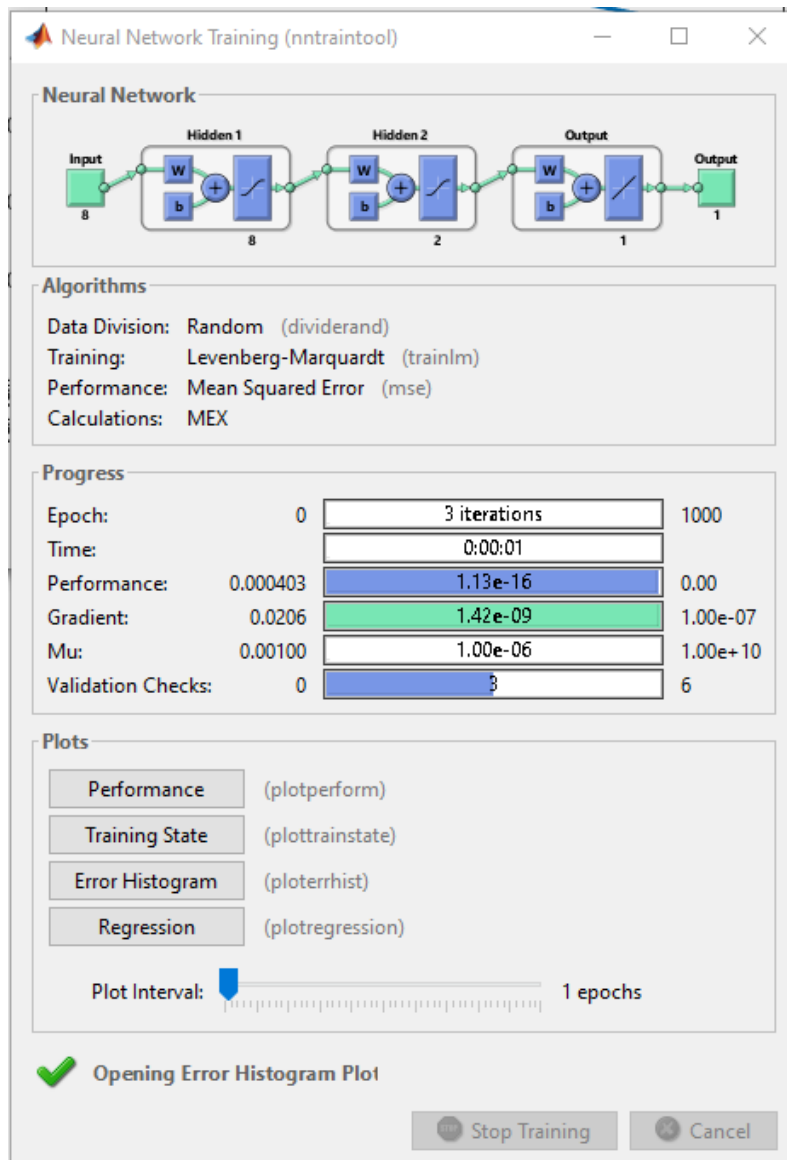
Figure 4.4 Neural network training for Flexural strength.

From Fig. 4.14, it is visible that the ANN predicted and experimental values of ΔR_a between initial, and final states conform with each other to a very high degree, with the maximum error equal to 5.14 %, and the other errors are negligible. Hence, it is certain that the developed ANN model has effectively learned the relationship between the input values and ΔR_a values, and thus can be used for maximizing the Flexural strength.
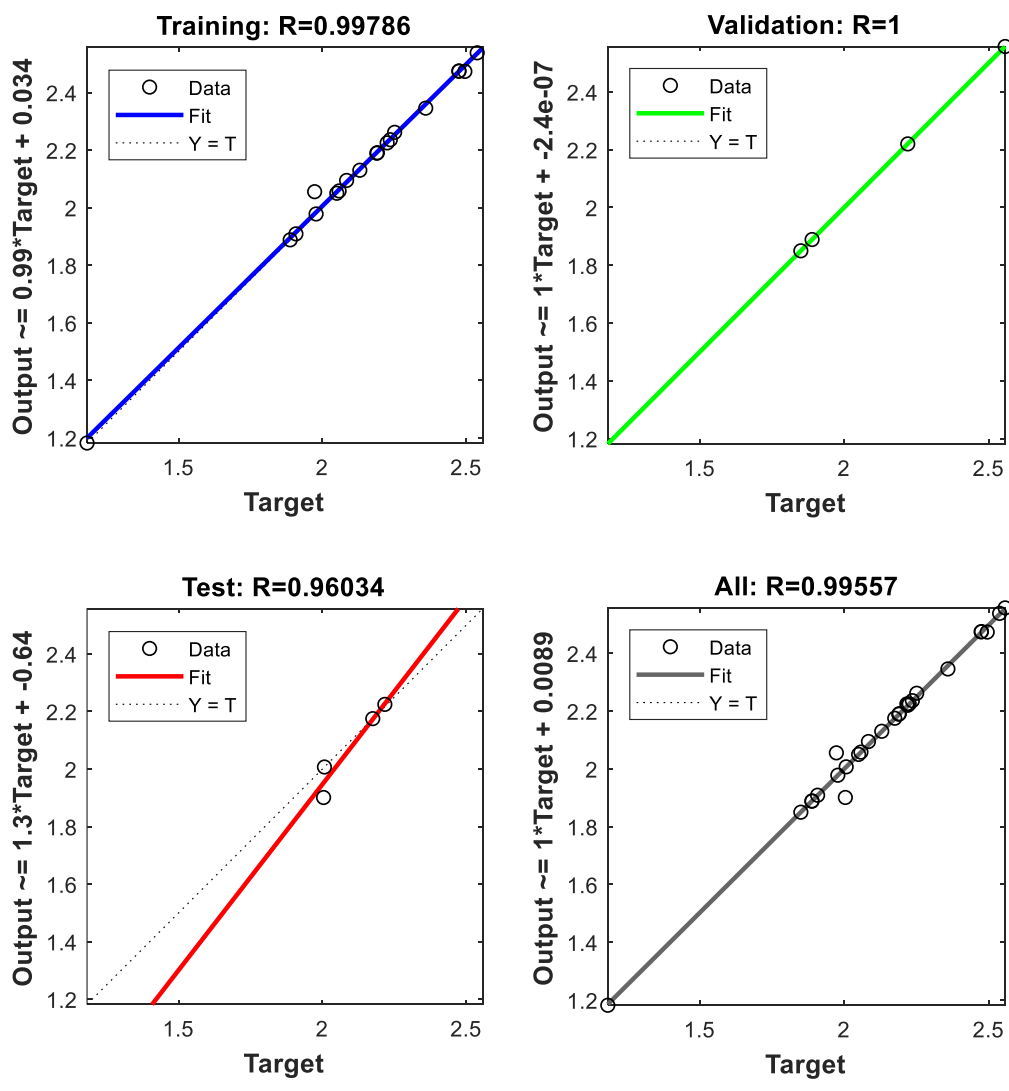
Figure 4.5 Regression Performance for trained ANN for Flexural strength.
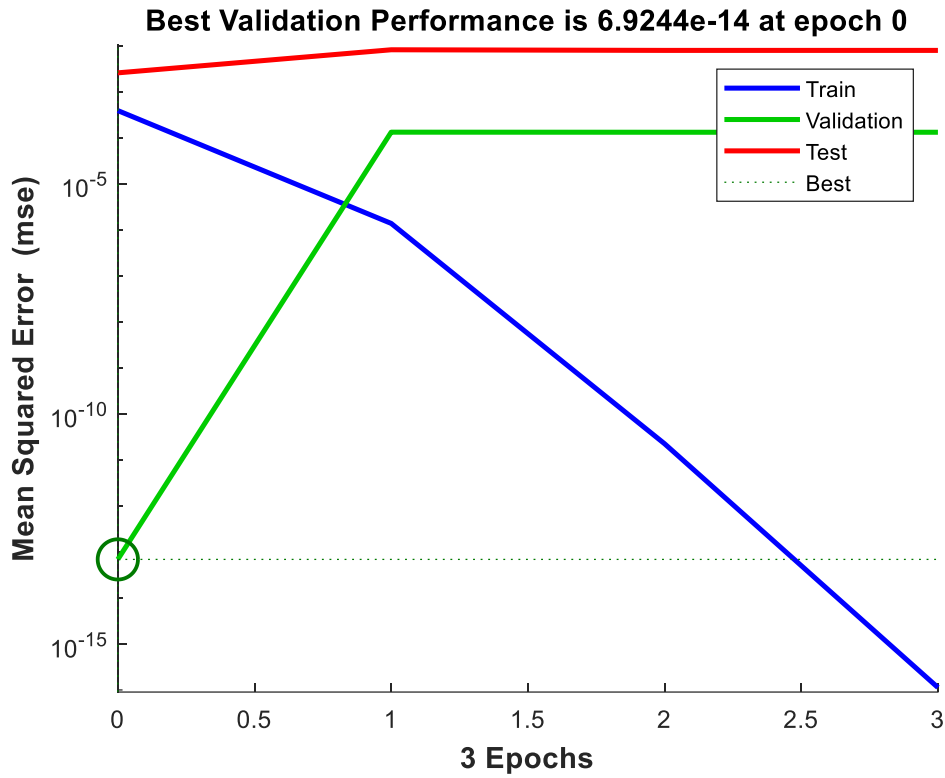
Figure 4.6 Variation of error with epochs for Flexural strength.
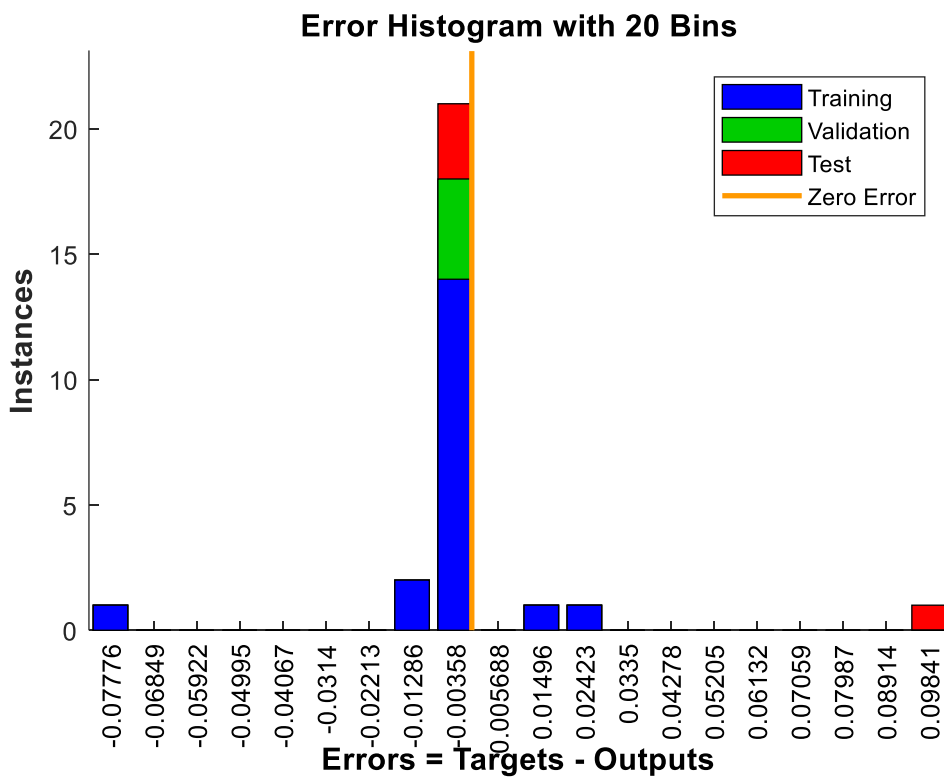
Figure 4.7 Error histogram plot for Flexural strength.
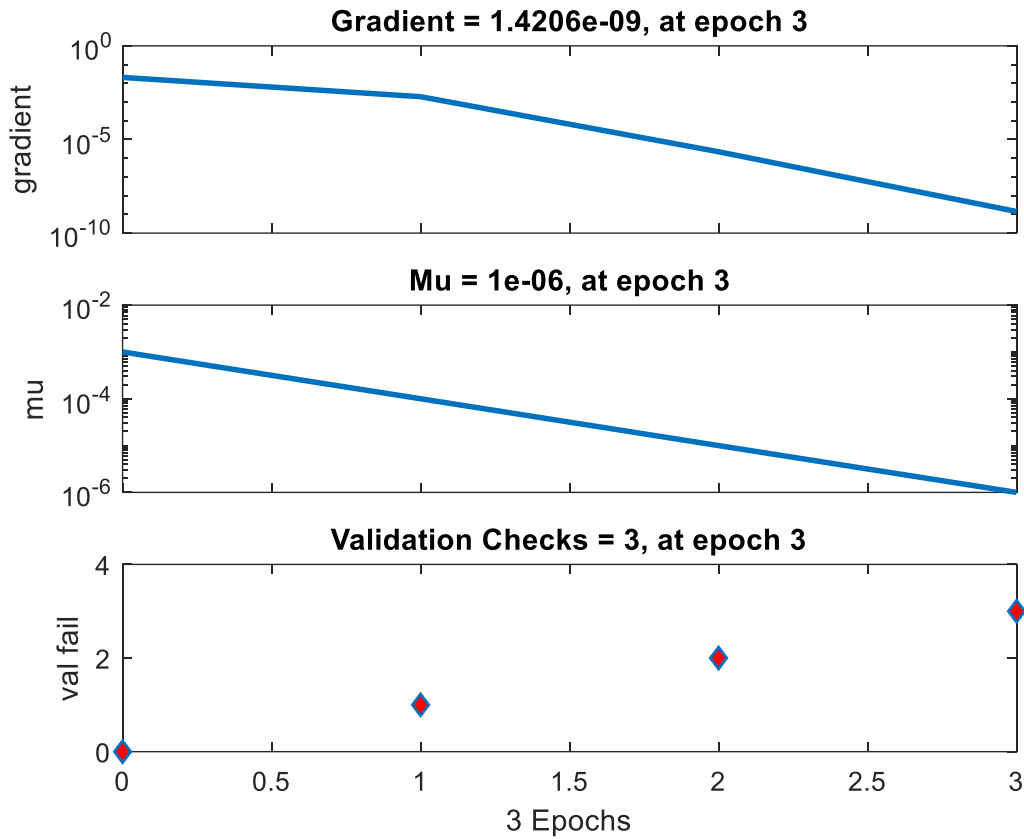
Figure 4.8 Training state of ANN for Flexural strength.

The trained ANN performance for 0.2% offset yield strength has been shown in Fig. 4.9, which tells the rationally good performance of trained ANN because the validation and test curves are on line, error histogram also confirms this fact in Fig. 4.12.

It cannot be ignored that the best validation performance has attained zero epoch with the value of $9.88*10^{-7}$, where the training persists until the 3rd epoch, Fig. 4.11, shows best validation performance. Fig. 4.13., shows the training state of ANN, where the gradient coefficient's final value is $1.5952*10^{-9}$, approximately zero at the 3rd epoch. Also, a diminishing value of gradient can be seen with the increase of epochs number. From Fig. 4.15, it is visible that the ANN predicted and experimental values of ΔR_a between initial, and final states conform with each other to a very high degree, with the maximum error equal to 1.25%, and the other errors are negligible. Hence, it is certain that the developed ANN model has

effectively learned the relationship between the input values and ΔR_a values, and thus can be used for maximizing the 0.2% offset yield strength.
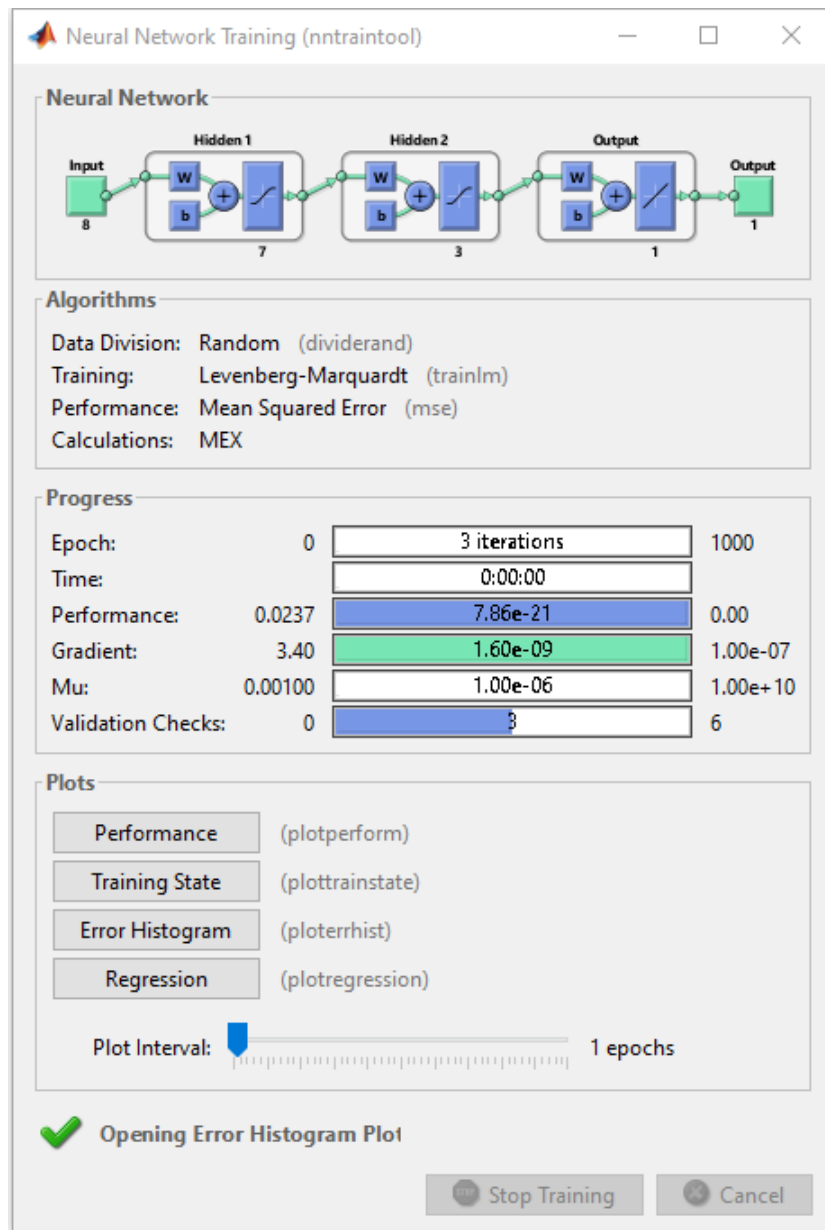
Figure 4.9 Neural network training for 0.2% offset yield strength.
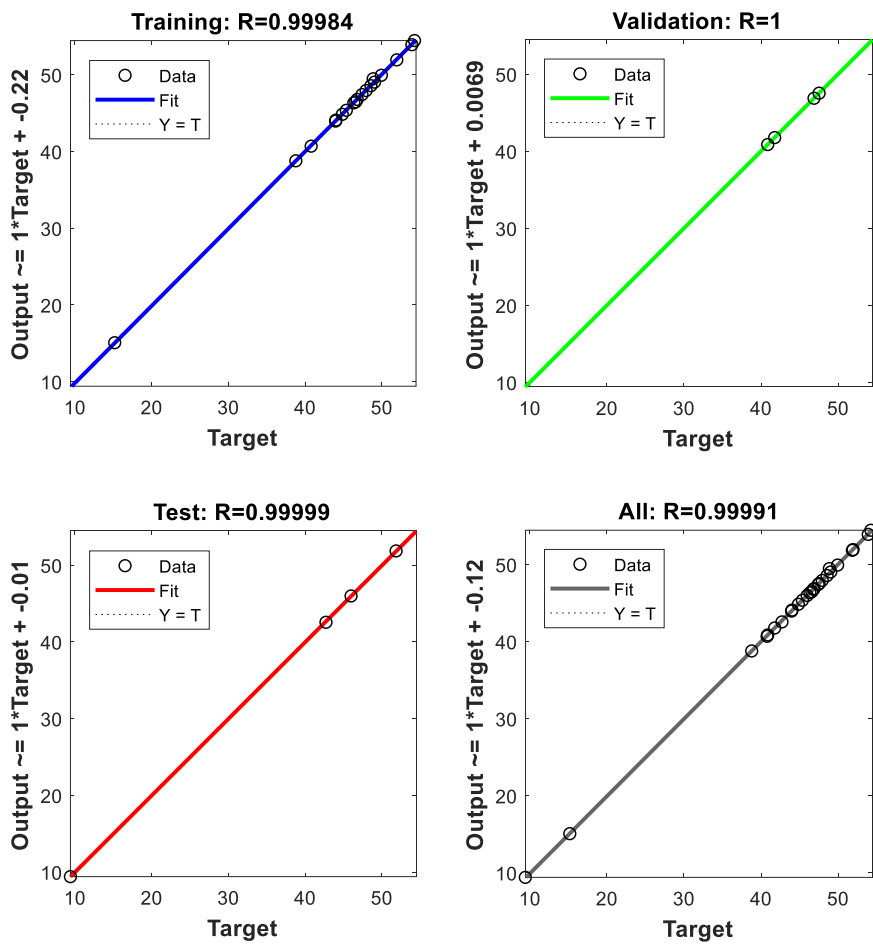
Figure 4.10 Regression Performance for 0.2% offset yield strength.
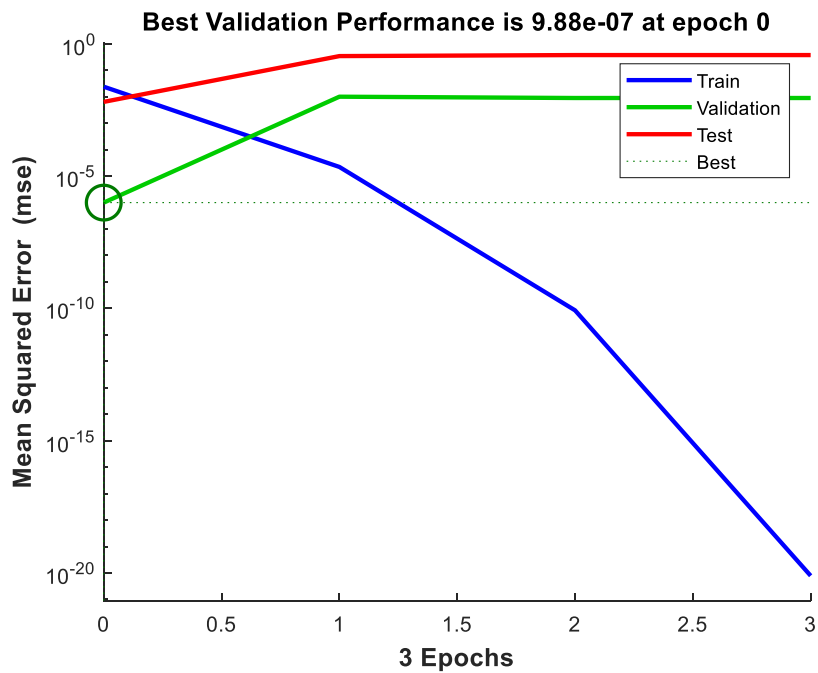
Figure 4.11 Variation of error with epochs for 0.2% offset yield strength.
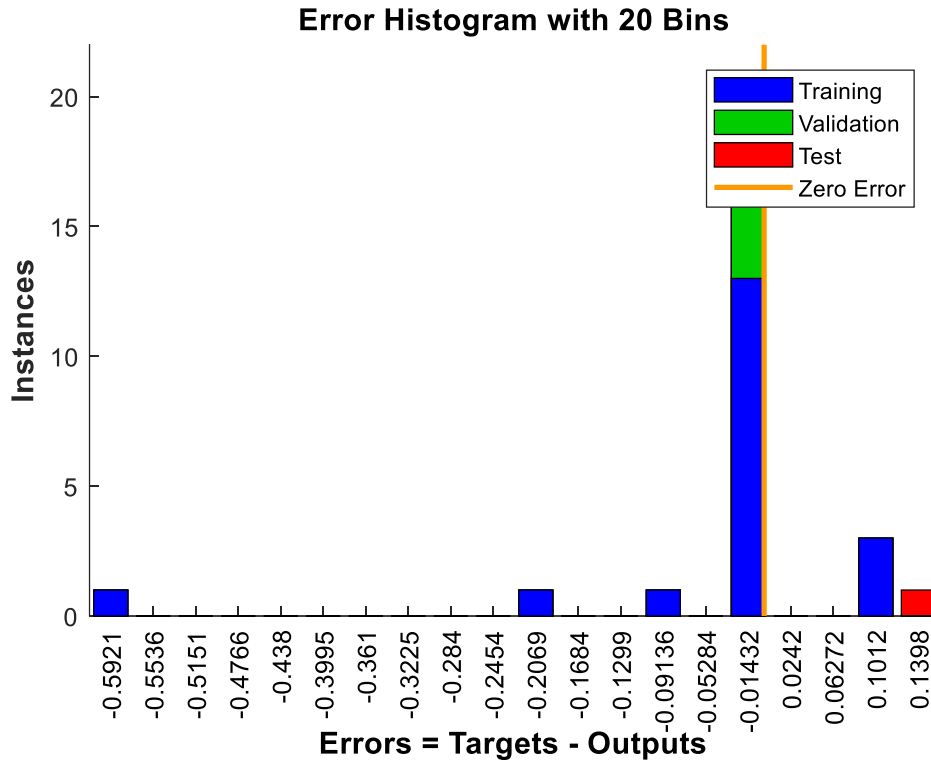
Figure 4.12 Error histogram plot for 0.2% offset yield strength.
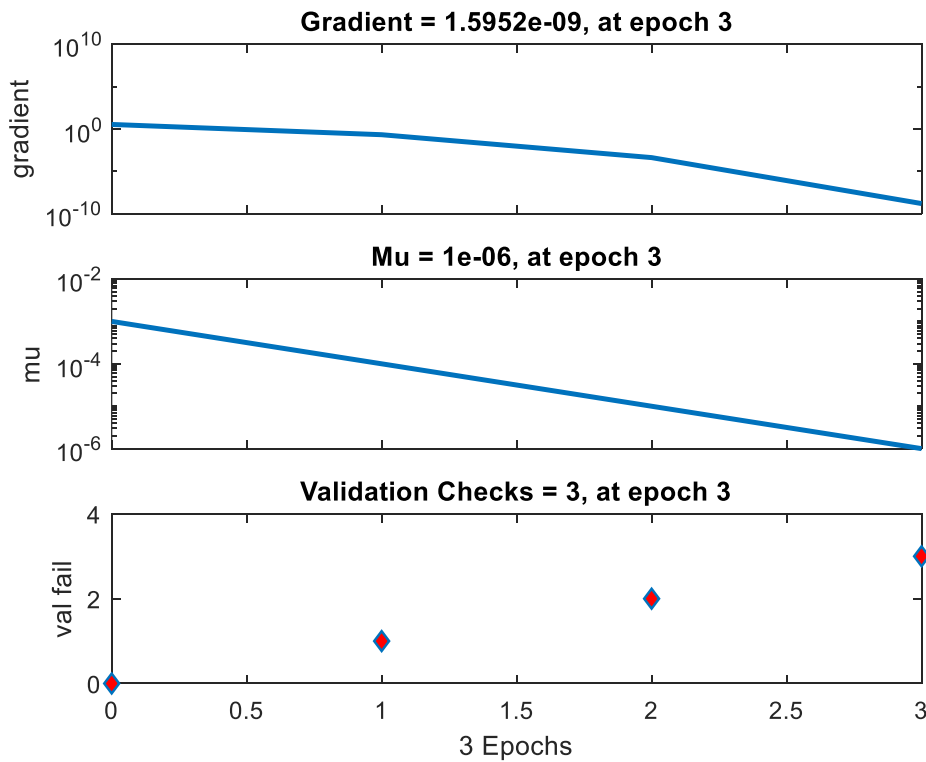
Figure 4.13 Training state of ANN for 0.2% offset yield strength.
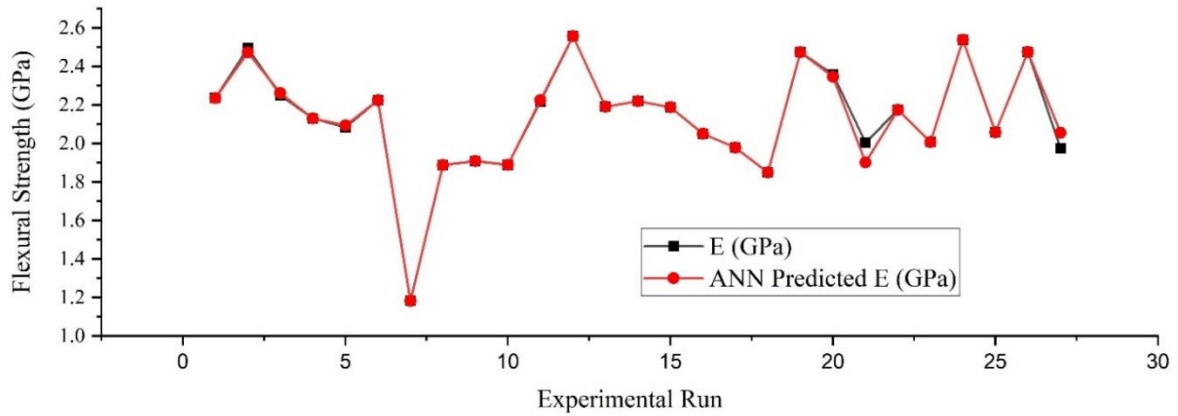
Figure 4.14 Comparison between experimental and ANN predicted 'E'.
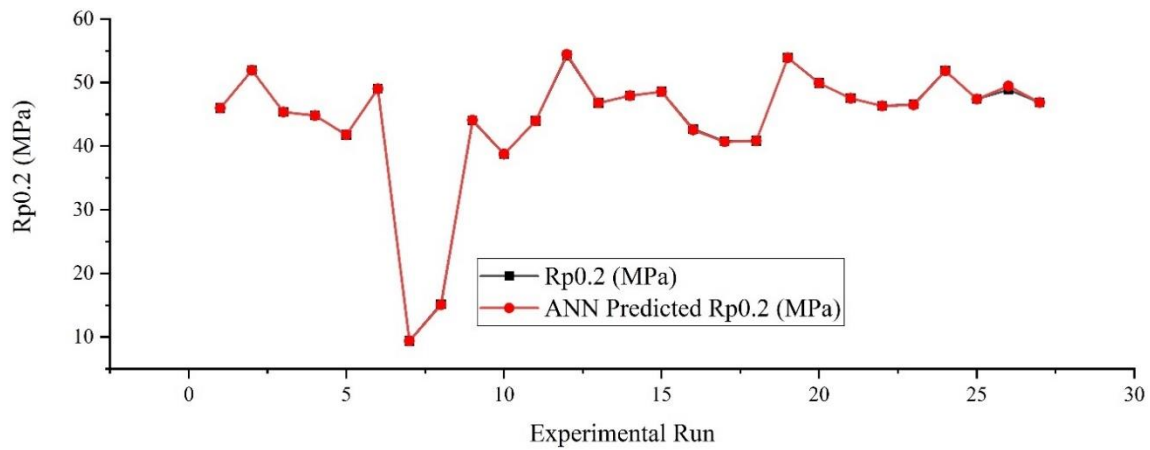
Figure 4.15 Comparison between experimental and ANN predicted '$R_{P0.2}$'.

The ANN predicted, and experimental values Flexural strength (E), and 0.2% offset yield strength ($R_{P0.2}$) comply to a very high degree with one another, and it is visible from **Figure 4.14**, and **Figure 4.15**. The maximum error out of 27 experimental runs comes out between ANN predicted and experimental values for E, and $R_{P0.2}$ equal to 5.14 %, and 1.25%, respectively. The weights and biases of the developed model are stored after confirming with this high degree of maximum error. ANN architecture presented in **Table 4** and the developed Neural Network architecture can be seen in **Figure 4.3**. The number of the hidden layers and the number of neurons in each hidden layer were chosen and then network efficiency was calculated by RMSE [31, 32]. The percentage error was measured as Equation (3) and the

values determined are shown in **Table 3**. It is therefore guaranteed that the relationship between the values of input and output has been effectively learned by the developed ANN model. It can thus be used to optimize the operation.

4.2 Genetic Algorithm

It is observed from the ANN models developed and from the literature that the output responses [77], such as the 'E' and '$R_{P0.2}$', are concurrent and harmonious in nature. Therefore, the multi-optimal combination of process parameters would satisfy the objectives [35, 36]. The Genetic Algorithm is able to offer better performance compared to traditional optimization techniques because of its robustness, independence of gradient knowledge, and usage of intrinsic parallelism in design space searches [79].

Genetic algorithm is a commercially viable, less complicated, and quicker for multi-objective optimization [79]. The optimization issue is resolved using this globally effective optimization method. GA is a search and exploration algorithm similar to the mechanism of natural selection that belongs to the class of evolutionary algorithm. GA optimizes the problems using strategies driven by replication, mutation, crossover (recombination) and selection phenomena [38, 39]. To this intent, the ANN models developed in MATLAB were coupled with GA.

Figure 4.16 describes the various steps involved in the implementation of the ANN-GA model. A random population of size '50' was initialized by taking (8–8-2-1), and (8–7-3-1) ANN models.

The experimental results conducted during the investigation are further used to develop a model of the 3d-printing process using artificial neural networks. The values of the output parameters obtained after carrying out each experiment in the design of the experiment table are given in **Table 5.**
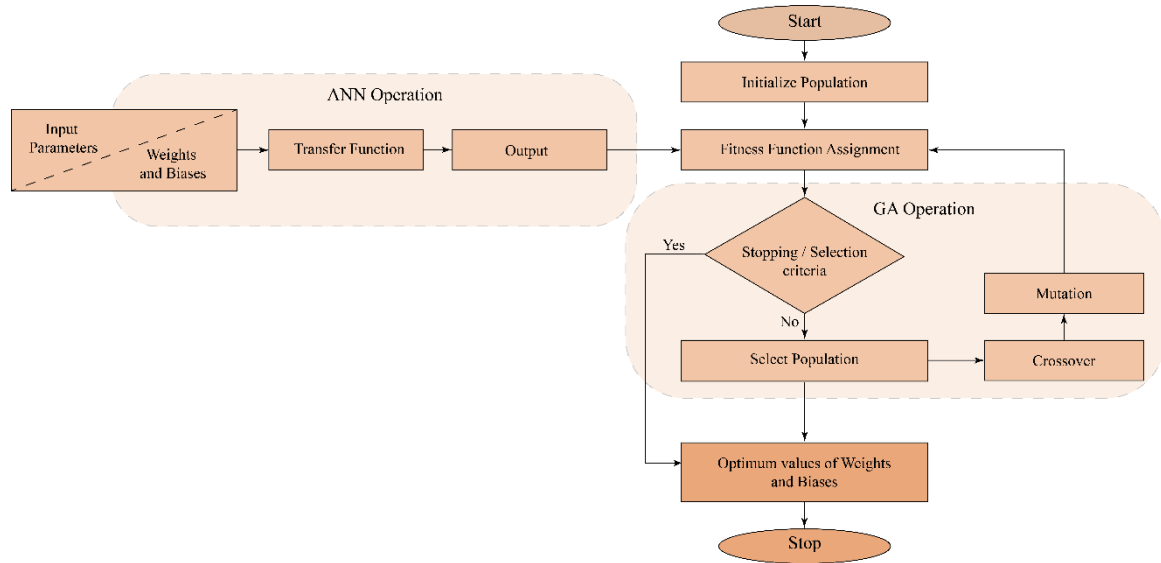
Figure 4.16 Schematic of ANN with GA process

The ANN models developed were used to predict the output for various input sets, and keeping other input parameters constant the influence of the input parameter on the output is observed. In this section the parametric analysis is summarized, whereas the findings of optimization and related discussion are outlined and followed by parametric analysis.

4.3 Parametric analysis using ANN

Here, the (8–8-2-1), and (8–7-3-1) ANN models developed for 'E' and '$R_{P0.2}$' respectively, are used to comprehend the consequence of input process variables- nozzle diameter, layer height, fill density, printing velocity, raster orientation and infill pattern on the outputs i.e., 'E' and '$R_{P0.2}$'.

4.3.1   Effect of Nozzle Diameter

Figure 4.17, illustrates the effect of different nozzle diameter values on 'E' and '$R_{P0.2}$'. It can be seen that as the nozzle diameter is incremented, the outputs 'E' decreases differently for all infill patterns. This may be attributed to the subsequent decrease in the layer matrix density when nozzle allows thicker fused ABS. While on increasing nozzle diameter, the '$R_{P0.2}$' value

affected differently for different infill patter, viz; it decreases for honey comb structure, increasing decreasing pattern for Linear infill pattern and a minute increment can be seen in rectilinear structure.
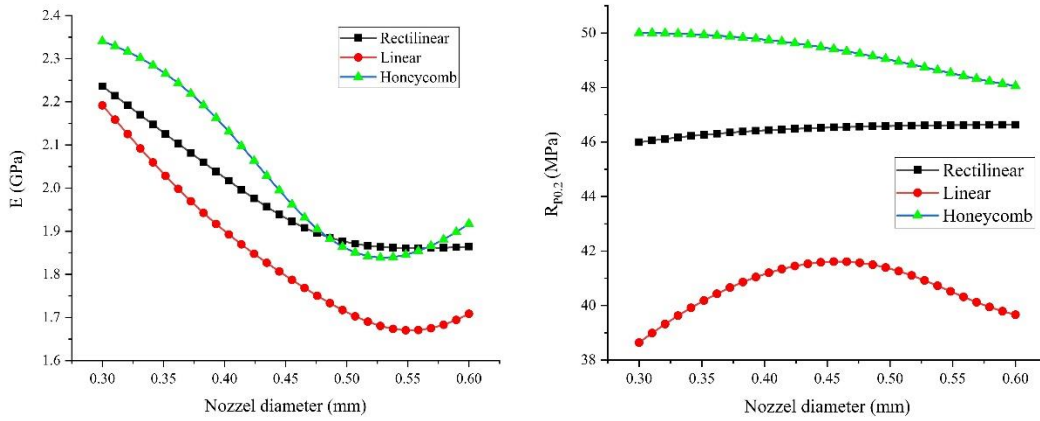
Figure 4.17 Effect of nozzle diameter on 'E' and '$R_{P0.2}$'.

4.3.2 Effect of Layer height

Figure 4.18, illustrates the effect of different layer height values on 'E' and '$R_{P0.2}$'. It can be seen that as the layer height is incremented, the outputs 'E' decreases differently for all infill patterns. It is seen that 'E' decrease with faster rates for honeycomb infill while it decreases comparatively with slower rates for rectilinear and linear infill patterns. This may be attributed to the subsequent decrease in the layer matrix density. While on increasing layer height, the '$R_{P0.2}$' values also decreasing for all the infill patterns. It can also be observed that on increasing the layer height with linear infill pattern, decreases the '$R_{P0.2}$' values with faster rates than the other two patterns.
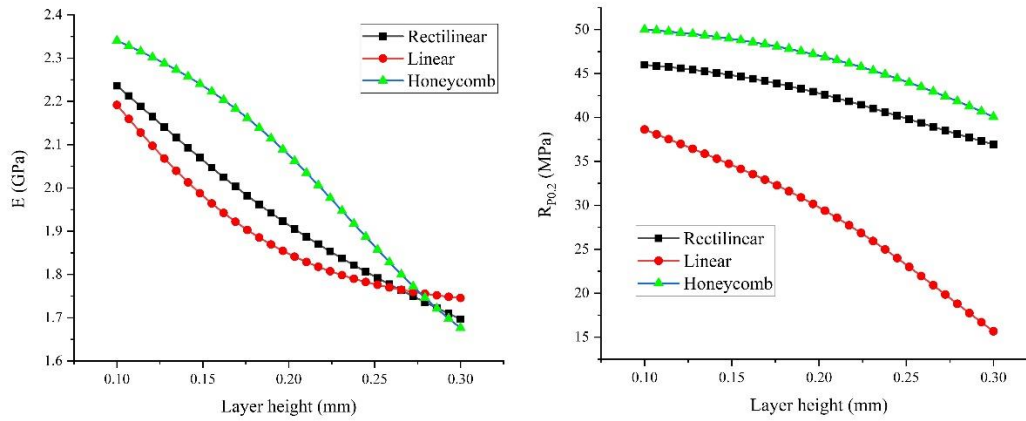
Figure 4.18 Effect of layer height on 'E' and '$R_{P0.2}$'.

4.3.3 Effect of Fill density

Figure 4.19, illustrates the effect of different fill density values on 'E' and '$R_{P0.2}$'. It can be seen that as the fill density is incremented, the outputs 'E' increases for all infill patterns. It increases for linear infill patter with faster rates than the other two infill patterns. The rate with which 'E' increases for honeycomb and rectilinear is almost same. While on increasing fill density the '$R_{P0.2}$' value affected differently for different infill patterns, viz; it affects negligible for honeycomb structure, increases with faster rate for linear than the increment rate showed by rectilinear pattern.
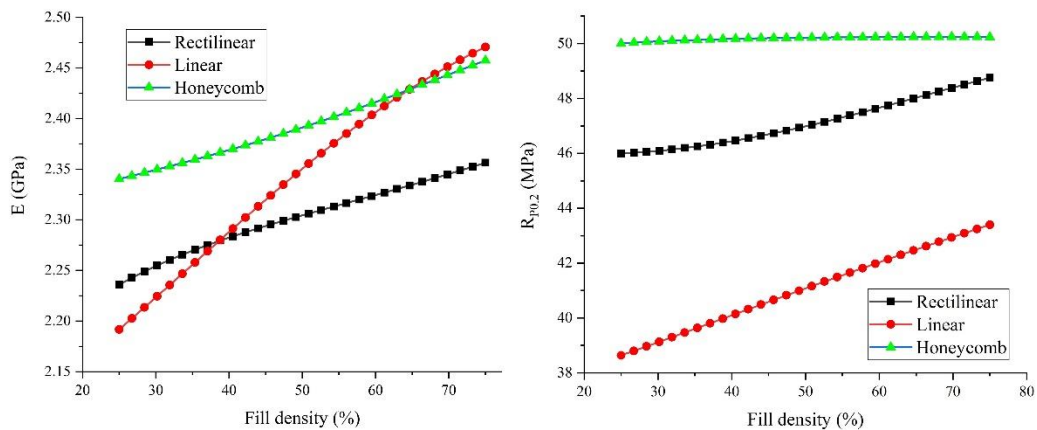
Figure 4.19 Effect of fill density on 'E' and '$R_{P0.2}$'.

4.3.4 Effect of Printing velocity

Figure 4.20, illustrates the effect of different printing velocity values on 'E' and '$R_{P0.2}$'. It can be seen that as the printing velocity is incremented, the outputs 'E' decreases differently for all infill patterns. It also can be seen that on increasing printing velocity more than 32 mm/s, the rate of decrement of 'E' printing velocity for rectilinear is more than linear infill pattern. Also, honeycomb infill pattern is not showing any considerable decrement. While on increasing printing velocity the '$R_{P0.2}$' value was affected differently for different infill patter, viz; it decreases for honey comb structure, increases for Linear infill pattern and a minute decrement can be seen in rectilinear structure.
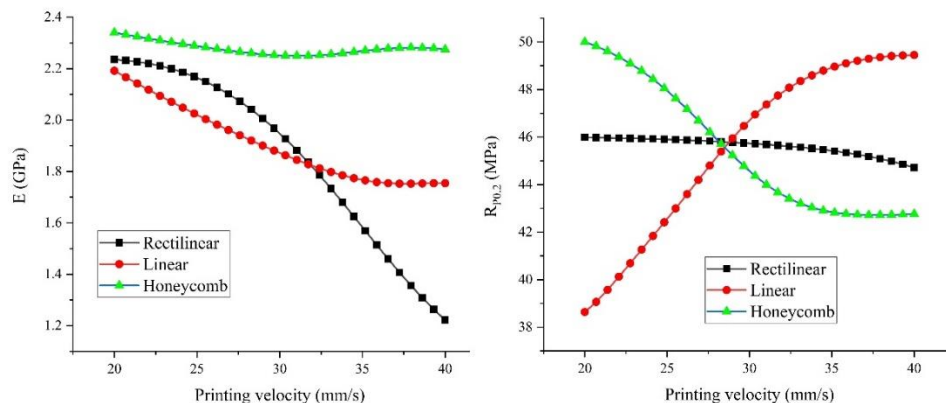
Figure 4.20 Effect of printing velocity on 'E' and '$R_{P0.2}$'.

4.3.5 Effect of Orientation

Figure 4.21, illustrates the effect of different orientation values on 'E' and '$R_{P0.2}$'. It can be seen that as the orientation is incremented, the outputs 'E' increases differently for all infill patterns. While on increasing orientation the '$R_{P0.2}$' value affected differently for different infill patter, viz; it decreases for honeycomb structure over the range, decreasing and increasing pattern for Linear infill pattern and an increment with slow growth can be seen in rectilinear structure.

44
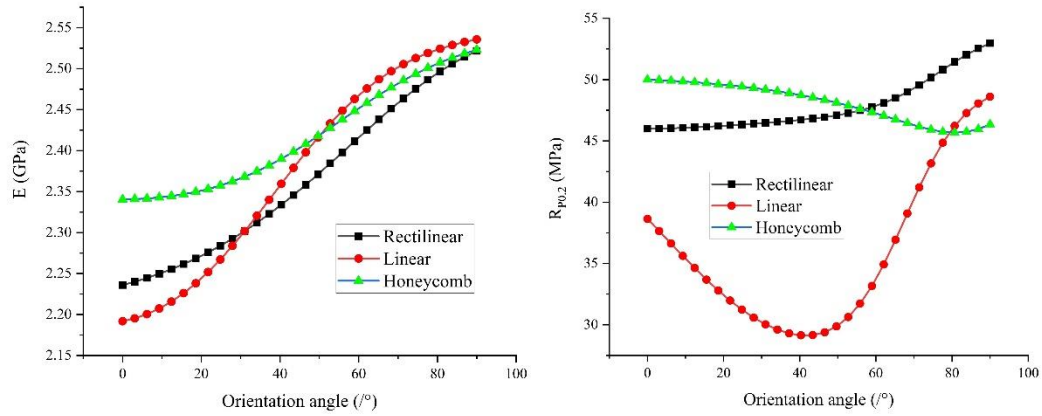
Figure 4.21 Effect of orientation on 'E' and 'R$_{P0.2}$'.

4.4 Multi-objective Optimisation using ANN-GA

To optimize (maximize) 'E' and 'R$_{P0.2}$' the developed ANN models are fed to a genetic algorithm program that calculates the value of each input parameter corresponding to the maximum output value achievable. These required goals were framed as objective functions, for optimizing the 3D printing process using GA. Furthermore, the developed ANN models were linked with GA, for the present bi-objective optimization. A GA program was coded, as per the objective, in MATLAB-17a for this purpose. The goals of the present research are to optimize 'E' and 'R$_{P0.2}$'. The objectives are as shown –

$$\text{Objective 1} = \text{Minimize } (1/E)$$

$$\text{Objective 2} = \text{Minimize } (1/ R_{P0.2})$$

The program is coded in MATLAB for the GA-based optimization of the ANN model as per objectives. During this optimization, GA was applied to the trained (8-8-2-1, and 8-7-3-1) ANN models for the determination of the objectives function. The ANN component is responsible for deciding the objective functions in the process of combined optimization by the ANN-GA model, while the GA aspect is responsible for ranking and sorting the ANN-based solution. The developed ANN models were provided the initial population of size 50 in the first iteration of optimization, the crossover rate, and the mutation rate is 0.8 and 0.01,

respectively. Selection parameters for GA operation have been enlisted in **Table 5**, and it is used in the subsequent iteration to measure the outputs viz. 'E' and '$R_{P0.2}$' for new offspring.

During optimization process, it is found that after 146 iterations, the optimum data are obtained. No noticeable improvement in process parameters was observed after that if the iterations reached 146 iterations. The Pareto fronts hence obtained were extracted for further analysis, and the optimal front of these 70 solutions are illustrated in **Figure 4.22**. Selected eight (including all coded different infill patterns) decision variables are bound by upper and lower limit as per restriction of 3D printer discussed, keeping in mind that all the responses have similar in nature as discussed.

Optimal solutions presented in Table 6 have decision variables. Optimized responses are compared with experimental values of responses in the subsections of this section. It may hence be concluded that the preference of one solution over another solely depends on the product specifications, processing capabilities resources, and the predilection of the process engineer. These 70 solutions have been presented in Table 6.

Table 5 List of GA parameters used.

Population Type	Crossover Fraction	Mutation Rate	Max. Generations	Initial Population
Double vector	0.8	0.01	146	50
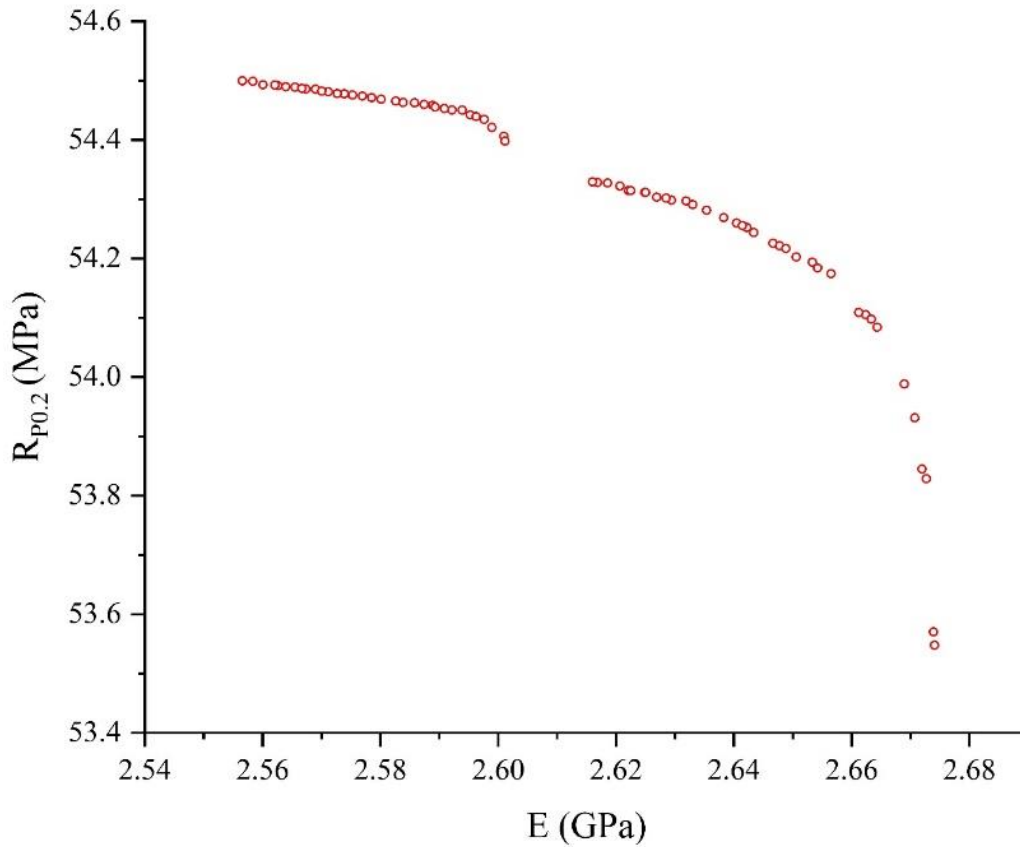
Figure 4.22 Pareto optimal front 'E' and '$R_{P0.2}$'.

Table 6 Set of optimal solution corresponding to inputs and outputs.

S. No	Nozzle diameter (mm)	Layer height (mm)	Fill density (%)	Printing velocity (mm/s)	Orientation (orient)	Rectilinear	Linear	Honey comb	E (GPa)	$R_{P0.2}$ (MPa)
1	0.53	0.10	63.98	21.14	86.31	0.79	0.48	0.18	2.557	54.50
2	0.59	0.10	64.14	21.19	86.13	0.97	0.61	0.13	2.589	54.46
3	0.59	0.10	64.20	21.18	86.23	0.94	0.62	0.15	2.587	54.46
4	0.60	0.10	64.66	26.92	85.80	0.41	0.02	0.47	2.629	54.30
5	0.60	0.10	64.63	29.54	85.23	0.17	0.15	0.51	2.674	53.55
6	0.58	0.10	64.64	21.14	86.32	0.90	0.50	0.20	2.574	54.48
7	0.60	0.10	64.68	28.26	85.27	0.26	0.03	0.47	2.669	53.99
8	0.56	0.10	64.36	21.14	86.33	0.89	0.50	0.19	2.567	54.49
9	0.60	0.10	64.63	26.38	85.85	0.42	0.03	0.44	2.617	54.33
10	0.60	0.10	64.65	27.69	85.62	0.36	0.03	0.48	2.651	54.20
11	0.60	0.10	64.49	27.02	85.29	0.36	0.02	0.47	2.643	54.24

12	0.60	0.10	64.66	26.92	85.80	0.41	0.02	0.47	2.632	54.30
13	0.60	0.11	62.08	21.74	86.08	0.99	0.86	0.02	2.601	54.41
14	0.60	0.10	64.63	26.52	85.65	0.41	0.03	0.47	2.625	54.31
15	0.60	0.10	63.51	21.48	86.17	0.99	0.61	0.11	2.595	54.44
16	0.60	0.10	64.66	26.90	85.74	0.41	0.02	0.48	2.629	54.30
17	0.60	0.11	62.96	21.40	86.14	0.99	0.81	0.05	2.599	54.42
18	0.58	0.10	64.23	21.33	86.25	0.95	0.56	0.13	2.584	54.46
19	0.60	0.10	64.63	26.39	85.72	0.42	0.02	0.39	2.616	54.33
20	0.60	0.10	64.62	27.76	85.48	0.35	0.02	0.47	2.654	54.18
21	0.53	0.10	64.08	21.14	86.32	0.83	0.48	0.19	2.558	54.50
22	0.60	0.10	64.66	27.13	85.54	0.39	0.03	0.48	2.638	54.27
23	0.58	0.10	64.37	21.17	86.22	0.95	0.60	0.17	2.583	54.47
24	0.55	0.10	64.01	21.14	86.30	0.85	0.51	0.18	2.563	54.49
25	0.55	0.10	63.96	21.15	86.31	0.85	0.48	0.19	2.562	54.49
26	0.60	0.10	64.64	26.64	85.81	0.42	0.03	0.44	2.622	54.31
27	0.60	0.10	64.64	26.44	85.83	0.42	0.03	0.44	2.619	54.33
28	0.60	0.10	62.80	21.67	86.19	0.99	0.66	0.11	2.596	54.44
29	0.56	0.10	64.23	21.13	86.28	0.89	0.51	0.19	2.569	54.49
30	0.58	0.10	64.14	21.18	86.13	0.97	0.61	0.13	2.586	54.46
31	0.55	0.10	64.43	21.19	86.17	0.81	0.52	0.16	2.560	54.49
32	0.60	0.10	64.55	26.98	85.53	0.37	0.02	0.47	2.642	54.25
33	0.60	0.10	64.58	26.60	85.58	0.40	0.02	0.41	2.627	54.30
34	0.60	0.10	64.58	27.05	85.67	0.37	0.02	0.47	2.640	54.26
35	0.55	0.10	64.16	21.15	86.29	0.88	0.51	0.17	2.565	54.49
36	0.60	0.10	64.65	26.66	85.69	0.38	0.03	0.46	2.635	54.28
37	0.59	0.10	64.17	21.35	86.21	0.97	0.63	0.10	2.592	54.45
38	0.60	0.10	64.66	27.75	85.33	0.30	0.03	0.46	2.662	54.11
39	0.53	0.10	63.98	21.14	86.31	0.79	0.47	0.18	2.557	54.50
40	0.58	0.10	64.11	21.17	86.28	0.94	0.53	0.18	2.580	54.47
41	0.57	0.10	64.06	21.14	86.23	0.92	0.50	0.17	2.573	54.48
42	0.59	0.10	64.15	21.23	86.24	0.97	0.60	0.08	2.591	54.45
43	0.60	0.10	64.64	27.43	85.55	0.37	0.03	0.47	2.647	54.23
44	0.58	0.10	64.19	21.17	86.18	0.93	0.57	0.16	2.579	54.47
45	0.55	0.10	64.10	21.16	86.28	0.89	0.51	0.16	2.567	54.49

46	0.56	0.10	64.26	21.17	86.26	0.91	0.52	0.16	2.571	54.48
47	0.57	0.10	64.25	21.18	86.21	0.94	0.55	0.16	2.577	54.47
48	0.60	0.10	64.57	27.29	85.37	0.36	0.03	0.47	2.648	54.22
49	0.58	0.10	64.51	21.15	86.31	0.90	0.52	0.19	2.575	54.48
50	0.60	0.10	64.66	27.58	85.53	0.33	0.03	0.48	2.657	54.17
51	0.60	0.10	64.64	27.76	85.48	0.29	0.04	0.47	2.664	54.08
52	0.60	0.10	64.67	29.02	85.21	0.21	0.04	0.49	2.673	53.83
53	0.60	0.10	64.43	27.03	85.41	0.37	0.02	0.46	2.641	54.26
54	0.60	0.10	62.44	21.39	86.15	1.00	0.68	0.04	2.598	54.43
55	0.60	0.10	64.60	28.19	85.58	0.33	0.03	0.44	2.661	54.11
56	0.60	0.10	64.53	26.53	85.88	0.42	0.02	0.42	2.621	54.32
57	0.60	0.10	64.67	26.49	85.74	0.41	0.02	0.46	2.622	54.31
58	0.56	0.10	63.98	21.13	86.29	0.90	0.52	0.18	2.570	54.48
59	0.60	0.10	64.64	27.31	85.61	0.35	0.03	0.47	2.649	54.22
60	0.60	0.10	64.66	26.43	85.73	0.37	0.02	0.46	2.633	54.29
61	0.60	0.10	64.62	28.32	85.48	0.25	0.06	0.49	2.671	53.93
62	0.60	0.10	64.62	27.27	85.55	0.33	0.03	0.47	2.653	54.19
63	0.60	0.10	64.64	27.76	85.48	0.30	0.04	0.47	2.663	54.10
64	0.60	0.10	64.66	29.03	85.21	0.22	0.04	0.49	2.672	53.84
65	0.60	0.11	62.08	21.72	86.09	1.00	0.87	0.03	2.601	54.40
66	0.60	0.10	64.63	26.52	85.65	0.41	0.03	0.48	2.625	54.31
67	0.56	0.10	64.01	21.15	86.30	0.85	0.51	0.18	2.564	54.49
68	0.60	0.10	64.63	29.55	85.23	0.17	0.14	0.51	2.674	53.57
69	0.59	0.10	64.23	21.24	86.23	0.97	0.61	0.13	2.589	54.46
70	0.59	0.10	64.10	21.21	86.24	0.98	0.66	0.08	2.594	54.45

4.4.1   Comparison of experimental and optimal 'E'

A comparison of experimental **'E'** values and the values found from Pareto optimal solution revealed that the maximum experimental value of **'E'** is 2.557 GPa at nozzle diameter = 0.4mm , layer height = 0.1mm, fill density = 75%, printing velocity = 20 mm/s, raster orientation = 90° and with rectilinear infill pattern (i.e., 100% effect of rectilinear and effect of linear and

honeycomb infill pattern was absent) as shown in experiment number 12 in Table 3. Whereas the maximum '**E**' obtained from optimal solution (Table 6) is 2.674 GPa at nozzle diameter = 0.6 mm, layer height = 0.1 mm, fill density = 64.63%, printing velocity = 29.54 mm/s, raster orientation = 85.23° (i.e., 85°13'48"). This optimised output depends on infill patterns and from Table 6, we can see the significance of rectilinear infill pattern is 0.17 (or 17%) for the attainment of same optimal flexural strength the significance of linear infill pattern and honeycomb are 0.15 and 0.51 respectively. It can be concluded from these results that minor change in input variables may increase the output by 4.57%. Furthermore, it can be seen that a combination of high nozzle diameter and infill density, small layer height and moderate printing velocity, is more suitable for achieving a higher '**E**'.

4.4.2   Comparison of experimental and optimal '$R_{P0.2}$'

An assessment of experimental '$R_{P0.2}$' values and the values found from Pareto optimal solution revealed that the maximum experimental value of '$R_{P0.2}$' is 54.26 MPa at nozzle diameter = 0.4mm , layer height = 0.1mm, fill density = 75%, printing velocity = 20 mm/s, raster orientation = 90° and with rectilinear infill pattern (i.e., 100% effect of rectilinear and effect of linear and honeycomb infill pattern was absent) as shown in experiment number 12 in Table 3. Whereas the maximum '$R_{P0.2}$' obtained from optimal solution (Table 6) is 54.50 MPa at nozzle diameter = 0.53 mm, layer height = 0.1 mm, fill density = 63.98%, printing velocity = 21.14 mm/s, raster orientation = 86.31° (i.e., 86°18'36"). This optimised output depends on infill patterns and from Table 6, we can see the significance of rectilinear infill pattern is 0.79 (or 79%) for the attainment of same maximum $R_{P0.2}$ the significance of linear infill pattern and honeycomb are 0.47 and 0.18 respectively. It can be concluded from these results that minor change in input variables may increase the output with confirmed optimised maximum.

Furthermore, it can be seen that a combination of high nozzle diameter and infill density, small layer height and small printing velocity, is more suitable for achieving a optimised '$R_{P0.2}$'.

4.5 Fractography

Microscopic studies of the specimens' cross-sections were carried out to confirm this observation. **Figure 4.23** displays the specimen with a honeycomb pattern at a density of 75% infill density. The brighter zones reflect the areas where the 3D printed beam was bent utilising three-point flexure testing. In terms of the acquired values for feedback (Table 3) and the fracture behaviour, it is clear that the specimen created by subsequent filaments has a larger ductility since these filaments have higher motility in comparison to the other. Strain hardening propagation can be clearly seen in discoloration of polymer in the **Figure 4.23** As a result, the crack growth feature that happens in the sample's outer fibre might reduce the ductility of injected parts, because these phenomena should continue for each layer of printed parts Similarly, the lower layer height and larger diameter of the nozzle aid in adhesion between successive layers. It can be observed that a combination of large nozzle diameter and infill density, a short layer height, and a moderate printing velocity is better for achieving a greater 'E' and '$R_{P0.2}$'. As a result, the maximum stress and flexural resistance of the printed specimens can be increased. Finally, printing the specimens with optimised parameters can result in greater resistance when subjected to bending forces.
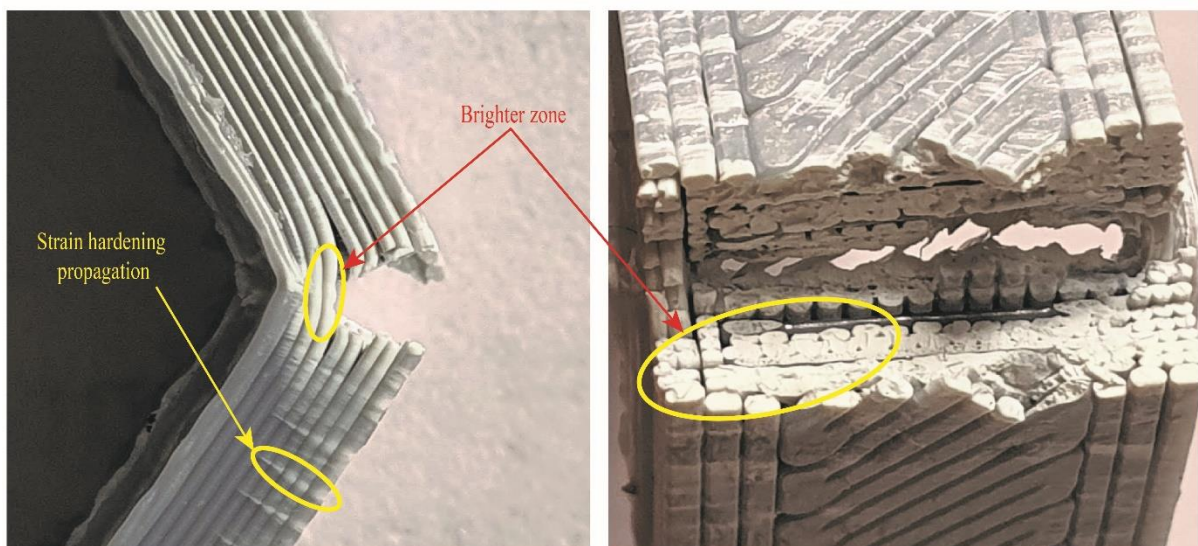

Figure 4.23 Fracture zone of ABS samples.

CONCLUSIONS

In this analysis, the Taguchi L27 orthogonal array was employed to build a set of experimental data that provides substantially better tolerance while using minimal test data. Six 3D printing parameters were chosen based on polymer needs for strength and lightweight. An artificial neural network model was employed to create a prediction model for 3D printed specimens, and the procedure was then optimised using a genetic algorithm.

1. The analysis demonstrate that the model makes reliable predictions and fits the test data well. Furthermore, the printing parameters have been optimised by simulating an experiment in order to enhance the performance of the 3D printed specimens and goods. It is observed that the ANN models could predict the behaviour of the output parameters with very high accuracy and efficiency. Upon further optimization with GA, the obtained ANN models were highly optimized and provided a better approach for the prediction of higher values of 'E' and '$R_{P0.2}$' than their experimental. ANN-GA-based modelling and optimization suggest a direct relation between choosing process parameters correctly and enhancing machining performance.

2. 'E' is inversely proportional to the nozzle diameter and layer height for all infill patterns. Also, 'E' is inversely proportional to the printing velocity but with lower significance nozzle diameter and layer height. It can be seen that 'E' is directly proportional to the fill density and orientation for all infill patterns.

3. '$R_{P0.2}$' is inversely proportional to the layer height for all infill patterns. While on increasing nozzle diameter, the '$R_{P0.2}$' value decreases for honeycomb structure, increasing decreasing pattern for Linear infill pattern and a minute increment can be seen in the rectilinear structure. While on increasing fill density the '$R_{P0.2}$' value

affected negligibly for honeycomb structure, increases with the faster rate for linear than the rectilinear pattern. While on increasing printing velocity the '$R_{P0.2}$' value decreases for honeycomb structure, increases for Linear infill pattern and a minute decrement was seen in the rectilinear structure. While on increasing orientation, the '$R_{P0.2}$' decreases for honeycomb structure over the range, decreasing and increasing pattern for Linear infill pattern and an increment with slow growth can be seen in the rectilinear structure.

4. The results suggest a multi-objective optimised setting of the 3D printer as presented in Table 6. Where the maximum flexural strength obtained from optimal solution (Table 6) is 2.674 GPa at nozzle diameter = 0.6 mm, layer height = 0.1 mm, fill density = 64.63%, printing velocity = 29.54 mm/s, raster orientation = 85.23° (i.e., 85°13'48"). This optimised output depends on infill patterns and from Table 6, we can see the significance of rectilinear infill pattern is 0.17 (or 17%) for the attainment of the same optimal flexural strength the significance of linear infill pattern and honeycomb are 0.15 and 0.51 respectively.

5. Also, the maximum '$R_{P0.2}$' obtained from optimal solution (Table 6) is 54.50 MPa at nozzle diameter = 0.53 mm, layer height = 0.1 mm, fill density = 63.98%, printing velocity = 21.14 mm/s, raster orientation = 86.31° (i.e., 86°18'36"). This optimised output depends on infill patterns and from Table 6, we can see the significance of rectilinear infill pattern is 0.79 (or 79%) for the attainment of the same maximum $R_{P0.2}$ the significance of linear infill pattern and honeycomb are 0.47 and 0.18 respectively.

6. Pareto's optimal front offers a set of optimal solutions (Table 6). The table acts as a convenient solution and facilitates a process engineer for the selection of the optimum values of control parameters depending on the product requirements.

Reference

[1] S. M. Yusuf and N. Gao, "Influence of energy density on metallurgy and properties in metal additive manufacturing," *Mater. Sci. Technol.*, vol. 33, no. 11, pp. 1269–1289, Jul. 2017, doi: 10.1080/02670836.2017.1289444.

[2] S. Moylan, J. Slotwinski, A. Cooke, K. Jurrens, and M. A. Donmez, "An Additive Manufacturing Test Artifact," *J. Res. Natl. Inst. Stand. Technol.*, vol. 119, p. 429, Oct. 2014, doi: 10.6028/jres.119.017.

[3] D. Mohan, Z. K. Teong, A. N. Bakir, M. S. Sajab, and H. Kaco, "Extending Cellulose-Based Polymers Application in Additive Manufacturing Technology: A Review of Recent Approaches," *Polymers*, vol. 12, no. 9, p. 1876, Aug. 2020, doi: 10.3390/polym12091876.

[4] D. Manfredi, F. Calignano, M. Krishnan, R. Canali, E. Ambrosio, and E. Atzeni, "From Powders to Dense Metal Parts: Characterization of a Commercial AlSiMg Alloy Processed through Direct Metal Laser Sintering," *Materials*, vol. 6, no. 3, pp. 856–869, Mar. 2013, doi: 10.3390/ma6030856.

[5] B. Vayre, F. Vignat, and F. Villeneuve, "Designing for Additive Manufacturing," *Procedia CIRP*, vol. 3, pp. 632–637, 2012, doi: 10.1016/j.procir.2012.07.108.

[6] R. V. Rao and D. P. Rai, "Optimization of fused deposition modeling process using teaching-learning-based optimization algorithm," *Eng. Sci. Technol. Int. J.*, vol. 19, no. 1, pp. 587–603, Mar. 2016, doi: 10.1016/j.jestch.2015.09.008.

[7] F. Calignano, T. Tommasi, D. Manfredi, and A. Chiolerio, "Additive Manufacturing of a Microbial Fuel Cell—A detailed study," *Sci. Rep.*, vol. 5, no. 1, p. 17373, Dec. 2015, doi: 10.1038/srep17373.

[8] T. Wohlers and T. Gornet, "History of additive manufacturing," p. 38, 2016.

[9]   P. Awasthi and S. S. Banerjee, "Fused deposition modeling of thermoplastic elastomeric materials: Challenges and opportunities," *Addit. Manuf.*, vol. 46, p. 102177, Oct. 2021, doi: 10.1016/j.addma.2021.102177.

[10]   R. Singh, S. Singh, and M. S. J. Hashmi, "Implant Materials and Their Processing Technologies," in *Reference Module in Materials Science and Materials Engineering*, Elsevier, 2016, p. B9780128035818041000. doi: 10.1016/B978-0-12-803581-8.04156-4.

[11]   J. Torres, J. Cotelo, J. Karl, and A. P. Gordon, "Mechanical Property Optimization of FDM PLA in Shear with Multiple Objectives," *JOM*, vol. 67, no. 5, pp. 1183–1193, May 2015, doi: 10.1007/s11837-015-1367-y.

[12]   S. K. Everton, M. Hirsch, P. Stravroulakis, R. K. Leach, and A. T. Clare, "Review of in-situ process monitoring and in-situ metrology for metal additive manufacturing," *Mater. Des.*, vol. 95, pp. 431–445, Apr. 2016, doi: 10.1016/j.matdes.2016.01.099.

[13]   X. Zhou and S.-J. Hsieh, "Thermal analysis of fused deposition modeling process using infrared thermography imaging and finite element modeling," Anaheim, California, United States, May 2017, p. 1021409. doi: 10.1117/12.2262796.

[14]   Z. Liu, Q. Lei, and S. Xing, "Mechanical characteristics of wood, ceramic, metal and carbon fiber-based PLA composites fabricated by FDM," *J. Mater. Res. Technol.*, vol. 8, no. 5, pp. 3741–3751, Sep. 2019, doi: 10.1016/j.jmrt.2019.06.034.

[15]   S. Belouettar, A. Abbadi, Z. Azari, R. Belouettar, and P. Freres, "Experimental investigation of static and fatigue behaviour of composites honeycomb materials using four point bending tests," *Compos. Struct.*, vol. 87, no. 3, pp. 265–273, Feb. 2009, doi: 10.1016/j.compstruct.2008.01.015.

[16]   A. Andrzejewska, Ł. Pejkowski, and T. Topoliński, "Tensile and Fatigue Behavior of Additive Manufactured Polylactide," *3D Print. Addit. Manuf.*, vol. 6, no. 5, pp. 272–280, Oct. 2019, doi: 10.1089/3dp.2017.0154.

[17] A. Peker *et al.*, "Additive manufacturing and biomechanical validation of a patient-specific diabetic insole," *Polym. Adv. Technol.*, vol. 31, no. 5, pp. 988–996, May 2020, doi: 10.1002/pat.4832.

[18] L. Aydin and S. Kucuk, "A method for more accurate FEA results on a medical device developed by 3D technologies," *Polym. Adv. Technol.*, vol. 29, no. 8, pp. 2281–2286, Aug. 2018, doi: 10.1002/pat.4339.

[19] M. Domingo-Espin, J. A. Travieso-Rodriguez, R. Jerez-Mesa, and J. Lluma-Fuentes, "Fatigue Performance of ABS Specimens Obtained by Fused Filament Fabrication," *Materials*, vol. 11, no. 12, p. 2521, Dec. 2018, doi: 10.3390/ma11122521.

[20] G. Gomez-Gras, R. Jerez-Mesa, J. A. Travieso-Rodriguez, and J. Lluma-Fuentes, "Fatigue performance of fused filament fabrication PLA specimens," *Mater. Des.*, vol. 140, pp. 278–285, Feb. 2018, doi: 10.1016/j.matdes.2017.11.072.

[21] J. A. Travieso-Rodriguez, M. D. Zandi, R. Jerez-Mesa, and J. Lluma-Fuentes, "Fatigue behavior of PLA-wood composite manufactured by fused filament fabrication," *J. Mater. Res. Technol.*, vol. 9, no. 4, pp. 8507–8516, Jul. 2020, doi: 10.1016/j.jmrt.2020.06.003.

[22] N. Guo and M. C. Leu, "Additive manufacturing: technology, applications and research needs," *Front. Mech. Eng.*, vol. 8, no. 3, pp. 215–243, Sep. 2013, doi: 10.1007/s11465-013-0248-8.

[23] A. Mohanty *et al.*, "Parametric optimization of parameters affecting dimension precision of FDM printed part using hybrid Taguchi-MARCOS-nature inspired heuristic optimization technique," *Mater. Today Proc.*, p. S2214785321045879, Jun. 2021, doi: 10.1016/j.matpr.2021.06.216.

[24] O. A. Mohamed, S. H. Masood, and J. L. Bhowmik, "Mathematical modeling and FDM process parameters optimization using response surface methodology based on Q-optimal

design," *Appl. Math. Model.*, vol. 40, no. 23–24, pp. 10052–10073, Dec. 2016, doi: 10.1016/j.apm.2016.06.055.

[25] R. K. Roy, *A primer on the Taguchi method*, 2nd ed. Dearborn, MI: Society of Manufacturing Engineers, 2010.

[26] S. Ahmad, R. M. Singari, and R. S. Mishra, "Modelling and optimisation of magnetic abrasive finishing process based on a non-orthogonal array with ANN-GA approach," *Trans. IMF*, vol. 98, no. 4, pp. 186–198, Jul. 2020, doi: 10.1080/00202967.2020.1776966.

[27] G. Candan and H. R. Yazgan, "Genetic algorithm parameter optimisation using Taguchi method for a flexible manufacturing system scheduling problem," *Int. J. Prod. Res.*, vol. 53, no. 3, pp. 897–915, Feb. 2015, doi: 10.1080/00207543.2014.939244.

[28] P. K. Gurrala and S. P. Regalla, "Part strength evolution with bonding between filaments in fused deposition modelling: This paper studies how coalescence of filaments contributes to the strength of final FDM part," *Virtual Phys. Prototyp.*, vol. 9, no. 3, pp. 141–149, Jul. 2014, doi: 10.1080/17452759.2014.913400.

[29] S. Ajith Arul Daniel, R. Pugazhenthi, R. Kumar, and S. Vijayananth, "Multi objective prediction and optimization of control parameters in the milling of aluminium hybrid metal matrix composites using ANN and Taguchi -grey relational analysis," *Def. Technol.*, vol. 15, no. 4, pp. 545–556, Aug. 2019, doi: 10.1016/j.dt.2019.01.001.

[30] D. N. Mondal, K. Sarangi, F. Pettersson, P. K. Sen, H. Saxén, and N. Chakraborti, "Cu─Zn separation by supported liquid membrane analyzed through Multi-objective Genetic Algorithms," *Hydrometallurgy*, vol. 107, no. 3–4, pp. 112–123, May 2011, doi: 10.1016/j.hydromet.2011.02.008.

[31] E. Deniz, O. Aydogmus, and Z. Aydogmus, "Implementation of ANN-based Selective Harmonic Elimination PWM using Hybrid Genetic Algorithm-based optimization," *Measurement*, vol. 85, pp. 32–42, May 2016, doi: 10.1016/j.measurement.2016.02.012.

[32] J. Giri, P. Shahane, S. Jachak, R. Chadge, and P. Giri, "Optimization of FDM process parameters for dual extruder 3d printer using Artificial Neural network," *Mater. Today Proc.*, vol. 43, pp. 3242–3249, 2021, doi: 10.1016/j.matpr.2021.01.899.

[33] B. N. Turner, R. Strong, and S. A. Gold, "A review of melt extrusion additive manufacturing processes: I. Process design and modeling," *Rapid Prototyp. J.*, vol. 20, no. 3, pp. 192–204, Apr. 2014, doi: 10.1108/RPJ-01-2013-0012.

[34] A. Dorigato, V. Moretti, S. Dul, S. H. Unterberger, and A. Pegoretti, "Electrically conductive nanocomposites for fused deposition modelling," *Synth. Met.*, vol. 226, pp. 7–14, Apr. 2017, doi: 10.1016/j.synthmet.2017.01.009.

[35] C. Liu, H. Qin, and P. T. Mather, "Review of progress in shape-memory polymers," *J. Mater. Chem.*, vol. 17, no. 16, p. 1543, 2007, doi: 10.1039/b615954k.

[36] S. H. Ahn, C. Baek, S. Lee, and I. S. Ahn, "Anisotropic Tensile Failure Model of Rapid Prototyping Parts - Fused Deposition Modeling (FDM)," *Int. J. Mod. Phys. B*, vol. 17, no. 08n09, pp. 1510–1516, Apr. 2003, doi: 10.1142/S0217979203019241.

[37] C. Casavola, A. Cazzato, V. Moramarco, and C. Pappalettere, "Orthotropic mechanical properties of fused deposition modelling parts described by classical laminate theory," *Mater. Des.*, vol. 90, pp. 453–458, Jan. 2016, doi: 10.1016/j.matdes.2015.11.009.

[38] K. Upadhyay, R. Dwivedi, and A. K. Singh, "Determination and Comparison of the Anisotropic Strengths of Fused Deposition Modeling P400 ABS," in *Advances in 3D Printing & Additive Manufacturing Technologies*, D. I. Wimpenny, P. M. Pandey, and L. J. Kumar, Eds. Singapore: Springer Singapore, 2017, pp. 9–28. doi: 10.1007/978-981-10-0812-2_2.

[39] B. M. Tymrak, M. Kreiger, and J. M. Pearce, "Mechanical properties of components fabricated with open-source 3-D printers under realistic environmental conditions," *Mater. Des.*, vol. 58, pp. 242–246, Jun. 2014, doi: 10.1016/j.matdes.2014.02.038.

[40] J. C. Snyder, C. K. Stimpson, K. A. Thole, and D. J. Mongillo, "Build Direction Effects on Microchannel Tolerance and Surface Roughness," *J. Mech. Des.*, vol. 137, no. 11, p. 111411, Nov. 2015, doi: 10.1115/1.4031071.

[41] J. C. Riddick, M. A. Haile, R. V. Wahlde, D. P. Cole, O. Bamiduro, and T. E. Johnson, "Fractographic analysis of tensile failure of acrylonitrile-butadiene-styrene fabricated by fused deposition modeling," *Addit. Manuf.*, vol. 11, pp. 49–59, Jul. 2016, doi: 10.1016/j.addma.2016.03.007.

[42] J. M. Chacón, M. A. Caminero, E. García-Plaza, and P. J. Núñez, "Additive manufacturing of PLA structures using fused deposition modelling: Effect of process parameters on mechanical properties and their optimal selection," *Mater. Des.*, vol. 124, pp. 143–157, Jun. 2017, doi: 10.1016/j.matdes.2017.03.065.

[43] R. van Weeren *et al.*, "Quality of Parts Processed by Fused Deposition," p. 8.

[44] D. Liao, L. Chen, J. Zhou, and R. Liu, "MODELING OF THERMAL STRESS DURING CASTING SOLIDIFICATION PROCESS," in *Engineering Plasticity and Its Applications*, Wuhan, China, May 2011, pp. 56–60. doi: 10.1142/9789814324052_0011.

[45] P. M. Pandey, N. V. Reddy, and S. G. Dhande, "Improvement of surface ®nish by staircase machining in fused deposition modeling," *J. Mater. Process. Technol.*, p. 9, 2003.

[46] M. A. Nazan, F. R. Ramli, M. R. Alkahari, M. A. Abdullah, and M. N. Sudin, "An exploration of polymer adhesion on 3D printer bed," *IOP Conf. Ser. Mater. Sci. Eng.*, vol. 210, p. 012062, Jun. 2017, doi: 10.1088/1757-899X/210/1/012062.

[47] L. R. Sbriglia, A. M. Baker, J. M. Thompson, R. V. Morgan, A. J. Wachtor, and J. D. Bernardin, "Embedding Sensors in FDM Plastic Parts During Additive Manufacturing," in *Topics in Modal Analysis & Testing, Volume 10*, M. Mains, Ed. Cham: Springer International Publishing, 2016, pp. 205–214. doi: 10.1007/978-3-319-30249-2_17.

[48] E. Macdonald *et al.*, "3D Printing for the Rapid Prototyping of Structural Electronics," *IEEE Access*, vol. 2, pp. 234–242, Dec. 2014, doi: 10.1109/ACCESS.2014.2311810.

[49] T. Rayna and L. Striukova, "From rapid prototyping to home fabrication: How 3D printing is changing business model innovation," *Technol. Forecast. Soc. Change*, vol. 102, pp. 214–224, Jan. 2016, doi: 10.1016/j.techfore.2015.07.023.

[50] J. Zaragoza-Siqueiros and H. I. Medellín-Castillo, "Design for Rapid Prototyping, Manufacturing and Tooling: Guidelines," in *Volume 2A: Advanced Manufacturing*, Montreal, Quebec, Canada, Nov. 2014, p. V02AT02A013. doi: 10.1115/IMECE2014-39310.

[51] L. Bian, S. M. Thompson, and N. Shamsaei, "Mechanical Properties and Microstructural Features of Direct Laser-Deposited Ti-6Al-4V," *JOM*, vol. 67, no. 3, pp. 629–638, Mar. 2015, doi: 10.1007/s11837-015-1308-9.

[52] Y. Jin, Y. He, G. Xue, and J. Fu, "A parallel-based path generation method for fused deposition modeling," *Int. J. Adv. Manuf. Technol.*, vol. 77, no. 5–8, pp. 927–937, Mar. 2015, doi: 10.1007/s00170-014-6530-z.

[53] C. Koch, L. Van Hulle, and N. Rudolph, "Investigation of mechanical anisotropy of the fused filament fabrication process via customized tool path generation," *Addit. Manuf.*, vol. 16, pp. 138–145, Aug. 2017, doi: 10.1016/j.addma.2017.06.003.

[54] G. C. Onwubolu and F. Rayegani, "Characterization and Optimization of Mechanical Properties of ABS Parts Manufactured by the Fused Deposition Modelling Process," *Int. J. Manuf. Eng.*, vol. 2014, pp. 1–13, Nov. 2014, doi: 10.1155/2014/598531.

[55] N. Mohan, P. Senthil, S. Vinodh, and N. Jayanth, "A review on composite materials and process parameters optimisation for the fused deposition modelling process," *Virtual Phys. Prototyp.*, vol. 12, no. 1, pp. 47–59, Jan. 2017, doi: 10.1080/17452759.2016.1274490.

[56] M. Mani, B. M. Lane, M. A. Donmez, S. C. Feng, and S. P. Moylan, "A review on measurement science needs for real-time control of additive manufacturing metal powder bed fusion processes," *Int. J. Prod. Res.*, vol. 55, no. 5, pp. 1400–1418, Mar. 2017, doi: 10.1080/00207543.2016.1223378.

[57] I. Cummings, E. Hillstrom, R. Newton, E. Flynn, and A. Wachtor, "In-Process Ultrasonic Inspection of Additive Manufactured Parts," in *Topics in Modal Analysis & Testing, Volume 10*, M. Mains, Ed. Cham: Springer International Publishing, 2016, pp. 235–247. doi: 10.1007/978-3-319-30249-2_20.

[58] Y. Tlegenov, Y. S. Wong, and G. S. Hong, "A dynamic model for nozzle clog monitoring in fused deposition modelling," *Rapid Prototyp. J.*, vol. 23, no. 2, pp. 391–400, Mar. 2017, doi: 10.1108/RPJ-04-2016-0054.

[59] H. Wu, Y. Wang, and Z. Yu, "In situ monitoring of FDM machine condition via acoustic emission," *Int. J. Adv. Manuf. Technol.*, Sep. 2015, doi: 10.1007/s00170-015-7809-4.

[60] F. Baumann, M. Schön, J. Eichhoff, and D. Roller, "Concept Development of a Sensor Array for 3D Printer," *Procedia CIRP*, vol. 51, pp. 24–31, 2016, doi: 10.1016/j.procir.2016.05.041.

[61] X. Zhou, S.-J. Hsieh, and Y. Sun, "Experimental and numerical investigation of the thermal behaviour of polylactic acid during the fused deposition process," *Virtual Phys. Prototyp.*, vol. 12, no. 3, pp. 221–233, Jul. 2017, doi: 10.1080/17452759.2017.1317214.

[62] C.-C. Kuo, W.-H. Chen, J.-F. Li, and Y.-J. Zhu, "Development of a flexible modeling base for additive manufacturing," *Int. J. Adv. Manuf. Technol.*, vol. 94, no. 1–4, pp. 1533–1541, Jan. 2018, doi: 10.1007/s00170-017-1028-0.

[63] S. Nuchitprasitchai, M. Roggemann, and J. Pearce, "Three Hundred and Sixty Degree Real-Time Monitoring of 3-D Printing Using Computer Analysis of Two Camera Views," *J. Manuf. Mater. Process.*, vol. 1, no. 1, p. 2, Jul. 2017, doi: 10.3390/jmmp1010002.

[64] N. Aliheidari, R. Tripuraneni, C. Hohimer, J. Christ, A. Ameli, and S. Nadimpalli, "The impact of nozzle and bed temperatures on the fracture resistance of FDM printed materials," Portland, Oregon, United States, Apr. 2017, p. 1016512. doi: 10.1117/12.2260105.

[65] R. Hashemi Sanatgar, C. Campagne, and V. Nierstrasz, "Investigation of the adhesion properties of direct 3D printing of polymers and nanocomposites on textiles: Effect of FDM printing process parameters," *Appl. Surf. Sci.*, vol. 403, pp. 551–563, May 2017, doi: 10.1016/j.apsusc.2017.01.112.

[66] C. Kousiatza, N. Chatzidai, and D. Karalekas, "Temperature Mapping of 3D Printed Polymer Plates: Experimental and Numerical Study," *Sensors*, vol. 17, no. 3, p. 456, Feb. 2017, doi: 10.3390/s17030456.

[67] D. Olivier, J. A. Travieso-Rodriguez, S. Borros, G. Reyes, and R. Jerez-Mesa, "Influence of building orientation on the flexural strength of laminated object manufacturing specimens," *J. Mech. Sci. Technol.*, vol. 31, no. 1, pp. 133–139, Jan. 2017, doi: 10.1007/s12206-016-1212-4.

[68] S. Ahmad, R. M. Singari, and R. S. Mishra, "Tri-objective constrained optimization of pulsating DC sourced magnetic abrasive finishing process parameters using artificial neural network and genetic algorithm," *Mater. Manuf. Process.*, pp. 1–15, Feb. 2021, doi: 10.1080/10426914.2020.1866196.

[69] R. K. Singh, S. Gangwar, D. K. Singh, and V. K. Pathak, "A novel hybridization of artificial neural network and moth-flame optimization (ANN–MFO) for multi-objective optimization in magnetic abrasive finishing of aluminium 6060," *J. Braz. Soc. Mech. Sci. Eng.*, vol. 41, no. 6, p. 270, Jun. 2019, doi: 10.1007/s40430-019-1778-8.

[70] C. M. Bishop, *Neural networks for pattern recognition*. Oxford university press, 1995.

[71] Muh. Ibnu Choldun R., J. Santoso, and K. Surendro, "Determining the number of hidden layers in neural network by using principal component analysis," in *Intelligent systems and applications*, Cham, 2020, pp. 490–500.

[72] M. K. Transtrum, B. B. Machta, and J. P. Sethna, "Geometry of nonlinear least squares with applications to sloppy models and optimization," *Phys. Rev. E*, vol. 83, no. 3, p. 036701, Mar. 2011, doi: 10.1103/PhysRevE.83.036701.

[73] M. A. Gluck and C. E. Myers, *Gateway to memory: an introduction to neural network modeling of the hippocampus and learning*. Cambridge, Mass: MIT Press, 2001.

[74] S. Shanmuganathan, "Artificial Neural Network Modelling: An Introduction," in *Artificial Neural Network Modelling*, S. Shanmuganathan and S. Samarasinghe, Eds. Cham: Springer International Publishing, 2016, pp. 1–14. doi: 10.1007/978-3-319-28495-8_1.

[75] B. Stojanović, A. Vencl, I. Bobić, S. Miladinović, and J. Skerlić, "Experimental optimisation of the tribological behaviour of Al/SiC/Gr hybrid composites based on Taguchi's method and artificial neural network," *J. Braz. Soc. Mech. Sci. Eng.*, vol. 40, no. 6, p. 311, Jun. 2018, doi: 10.1007/s40430-018-1237-y.

[76] R. N. Yadav, V. Yadava, and G. K. Singh, "Multi-objective optimization of process parameters in Electro-Discharge Diamond Face Grinding based on ANN-NSGA-II hybrid technique," *Front. Mech. Eng.*, vol. 8, no. 3, pp. 319–332, Sep. 2013, doi: 10.1007/s11465-013-0269-3.

[77] L. Chen, A. Ahadi, J. Zhou, and J.-E. Ståhl, "Modeling Effect of Surface Roughness on Nanoindentation Tests," *Procedia CIRP*, vol. 8, pp. 334–339, 2013, doi: 10.1016/j.procir.2013.06.112.

[78] S. H. R. Pasandideh and S. T. A. Niaki, "Multi-response simulation optimization using genetic algorithm within desirability function framework," *Appl. Math. Comput.*, vol. 175, no. 1, pp. 366–382, Apr. 2006, doi: 10.1016/j.amc.2005.07.023.

[79] S. Datta, C. Garai, and C. Das, "Efficient Genetic Algorithm On Linear Programming Problem For Fittest Chromosomes," *J. Glob. Res. Comput. Sci.*, vol. 3, no. 6, p. 8, 2012.

[80] A. Ghosh and S. Tsutsui, *Advances in Evolutionary Computing Theory and Applications*. Berlin: Springer Berlin, 2013.

[81] K. Deb, *Multi-objective optimization using evolutionary algorithms*, vol. 16. John Wiley & Sons, 2001.